GROWTH AND OPTICAL CHARACTERIZATION OF INDIUM OXIDE (InO$_X$) AND ZINC OXIDE (ZnO) FILMS

Undergraduate Thesis

Sotirios Panagou

Supervisor: **Kiriakidis George, Associate Professor Physics Dpt. Univ.**

Physics Department

University of Crete

Heraclion, Crete, Greece

2015

CONTENTS

Acknowledgements

Mr. George Kyriakidis for his guidance, help and patience throughout this project.

Mr. Eleutherios Iliopoulos for his guidance and help with the spectroscopic ellipsometry measurement.

Ioannis Kortidis for his help with constructing the samples, patience in answering my endless questions and guidance for the duration of the project.

Mr. Aperathitis Elias for his help with the measurement of the thickness of the films using A-step technique.

ABSTRACT

Indium Oxide and Zinc Oxide thin films have been prepared by reactive dc magnetron sputtering in oxygen plasma, using metallic In or Zn targets respectively. Films were deposited onto Corning 1707F low alkali glass substrates.

Transmission spectrum has been obtained by UV/Vis spectroscopy, in order to determine the optical constants in a variety of thickness (600 – 1600 nm) and optical band gaps. For Indium oxide, refractive index had an average value of 1.99, the energy band gap was found to be 3.5±0.05 eV and its lattice permittivity in the region of 3.6 – 4.3. For Zinc Oxide, refractive index had an average value of 1.89, the energy band gap was found to be 3.21±0.05 eV and its lattice permittivity in the region of 3.3 – 3.8.

Spectroscopic Ellipsometry measurements have been made on ZnO thin films with a variety of thicknesses (200 nm, 250nm), in order to create a model for the fitting of the measured values and evaluate the optical constants, thickness and their complex dielectric function.

ABSTRACT

Χρησιμοποιώντας dc magnetron εναπόθεση σε υπόστρωμα corning glass (Corning 1707F low alkali) με μεταλικούς στόχους In και Zn ετοιμάσαμε λεπτά υμένια οξειδίου του Ινδίου και οξειδίου του Ψευδάργυρου

Χρησιμοποιώντας φασματόμετρο UV/VIS πήραμε το φάσμα διάδοσης, έτσι ώστε να υπολογίσουμε τις οπτικές σταθερές των λεπτών υμενίων σε διαφορετικά πάχη καθώς και τον υπολογισμό του ενεργειακού χάσματος. Για το οξείδιο του Ινδίου, ο δείκτης διάθλασης είχε μέση τιμή 1.99 με ενεργειακό χάσμα στην περιοχή των 3.5 eV. Για το οξείδιο τον ψευδαργύρου, ο δείκτης διάθλασης είχε μέση τιμή 1.89 με ενεργειακό χάσμα στην περιοχή των 3.3 eV.

Χρησιμοποιήσαμε φασματοσκοπία ελλειψομέτρου σε λεπτά υμένια οξειδίου του Ψευδαργύρου (200nm, 250nm), για την δημιουργία κεντρικού μοντέλου υπολογισμού οπτικών σταθερών, πάχους καθώς και της διηλεκτρικής σταθεράς.

1. Introduction

Zinc oxide (ZnO) and Indium oxide (In_2O_3) are both of the metal oxide family. They are both transparent semiconducting materials. Indium oxide has a wide direct optical band gap (3-4 eV) with high transparency in the visible light range and high reflectivity in the near IR light range. Indium oxide transparent thin films can be used as transparent electrodes in electronic and optoelectronic devices (solar cells, flat panel displays). Zinc Oxide is known to have a wide bandgap in the region of 3.2 eV and a high exciton binding energy, in the region of 60 meV. This combination is making it useful in the growth of high quality crystals as well as blue optical devices (Blue LED).

Zinc oxide and Indium oxide thin semiconducting films can be deposited using several techniques such as: dc and rf sputtering, reactive evaporation, chemical vapor deposition, spray pyrolysis, molecular beam epitaxial. In all of these methods, deposition is made with oxygen as background atmosphere. Oxygen is the reason that conductivity of these films arises, due to the excess of electrons of charged oxygen vacancies in the crystal structure of both crystals.

Optical properties of zinc oxide and indium oxide can be studied by using a transmission spectrometer; region of the wavelengths measured is from 200 nm (UV region) to 1000 nm (NIR). By acquiring the transmission spectrum of the thin films the thickness d can be determined. Optical constants such as: refractive index n, extinction coefficient k, as well as complex dielectric function ε and energy band gap can also be calculated using Fresnel coefficients or the Manifacier equations [27]. Thickness calculated by the transmission spectrum can be compared with the thickness obtained by using the stylus profilometer.

Spectroscopic ellipsometry measurements can be done for thin films of low thickness (200 nm – 550 nm); with the spectrum obtained many parameters of the thin films can be calculated, such as its optical constants and thickness. Modeling of structure and optical constants is made during the fitting process of the samples.

The aim of this thesis is to study the optical properties of semiconducting zinc oxide and indium oxide thin films prepared by reactive dc magnetron sputtering at room temperature. This thesis is divided into 5 chapters. Introduction is Chapter 1. Chapter 2 is divided into 2 sections. In section 2.1, natural structure of In_2O_3 and ZnO is described. In section 2.2, Stoichiometry and non-stoichiometry as well as oxygen vacancies are described. In chapter 3, experimental techniques and methods which have been used for the growth and characterization of our films, are described in detail. In chapter 4, experimental results of the characterization are presented in sections, each followed by a discussion. In Chapter 5, a general conclusion of this thesis is presented.

2. Current status of In_2O_3 and ZnO

2.1 Natural Structure of In_2O_3 and ZnO

2.1.1 In_2O_3

In_2O_3 belongs to the metal sesquioxides family, M_2O_3. Crystallization formation for this family is of the corundum type and has 3 modifications, the A, B and C rare earth structure. Corundum type A modification is trigonical, B modification is monoclinic and C modification is cubic. Crystal structure of Indium Oxide has the C-type rare earth structure, known since the early beginning of 20th century and has been refined by x-ray diffraction [1-3]. Crystal structure is body-centered cubic with 80 atoms per unit cell (respecting the 2/3 cation/anion ratio), 32 are metallic atoms (Indium), from which 8 In(1) are at the b site and the remaining 24 In(2) at the d site, and the remaining 48 are oxygen atoms positioned at e sites [4]. There are two structural arrangements in the crystal, Indium atoms coordinated by 6 oxygen atoms forming a tetrahedron while oxygen atoms coordinated by 4 indium atoms forming a tetrahedron, as shown in Fig 2.1. Neighboring structural arrangements share their edges and corners.
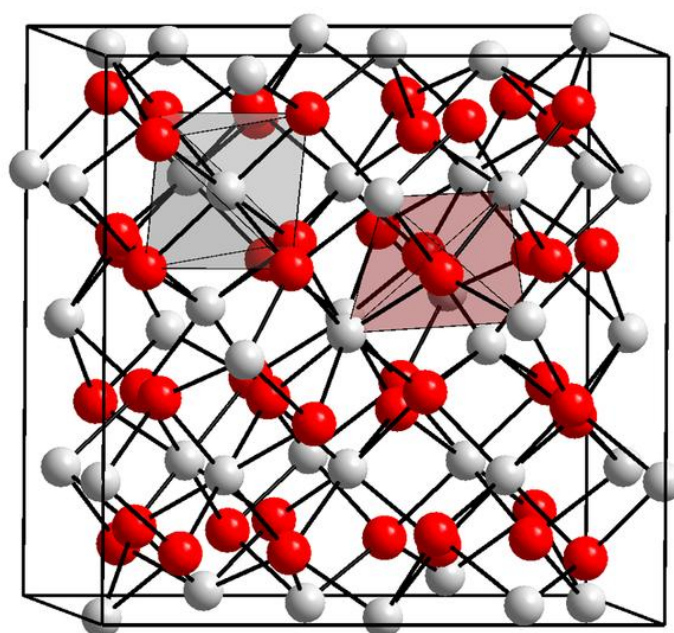
Fig. 2.1 *Unit Cell of In_2O_3*

The C modification structure is similar to fluorite structure. According to the fluorite structure, the lattice of the In_2O_3 is formed by a cubic face centered indium sublattice, three quarters of tetrahedron vacancies between indium atoms are occupied by oxygen atoms while the remaining one quarter is empty. Every fourth anion is missing so there are anion shifts in its place.

Marezio [2] carried out X-ray diffraction analysis on In_2O_3 single crystals and proved that there are two non-equivalent crystallographic indium atoms and only one oxygen atom. Coordination arrangement can be seen in **Fig. 2.2**
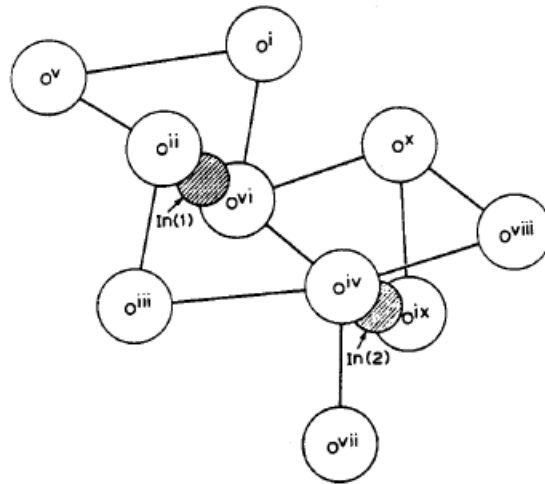
*Fig. 2.2 Indium Oxide atom coordination [2]*

2.1.2 ZnO

Zinc Oxide has been widely studied since 1935 **[5]** and is still critical in our day-to-day life through industry. Interest in this material is highly arisen lately by the development of growth technologies for producing high quality crystals and epitaxial layers.

Zinc Oxide has a wide bandgap, of about 3.4 eV and a large exciton binding energy, in the region of 60 meV at room temperature making ZnO important for blue and ultra-violet optical devices. Although it is still difficult for ZnO to be doped as p-type, stated by Alex Zunger *et al* and Hosono *et al,* efforts are being made to overcome this and allow the development of it **[6]**.

At ambient pressure and temperature, ZnO crystallizes in the wurtzite structure as shown in **Fig. 2.3**.

ra
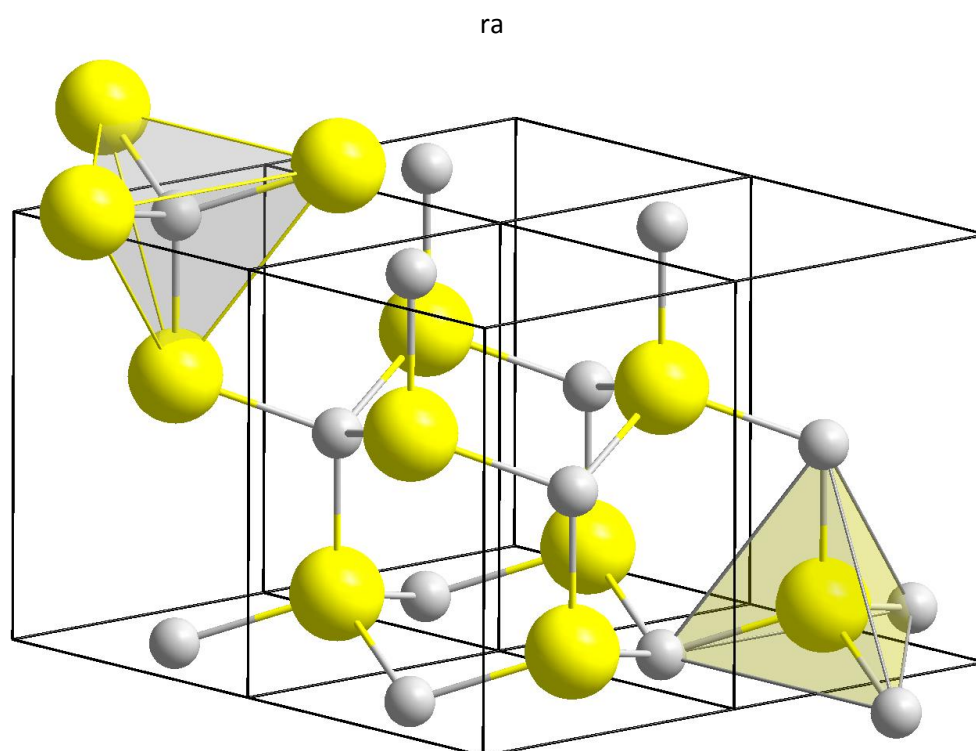
Fig. 2.3 *Zinc Oxide Wurtzite structure*

Wurtzite structure, is a hexagonal lattice, and is characterized by two interconnecting sublattices of Zn^{2+} and O^{2-}, in a way that each Zn ion is surrounded by a tetrahedral of oxygen ions. With this tetrahedral coordination, a polar symmetry is achieved along the hexagonal axis. This polarization gives to ZnO numerous of its properties, including its piezoelectricity and spontaneous polarizations, and also helps in its crystal growth as well as etching and defect generation. The four common face terminations of wurtzite ZnO are the polar Zn terminated (0001) and O terminated

(000.1) faces (c-axis oriented), and the non polar (11.20) (a-axis) and (10.10) faces that contains equal Zn and O atoms [7].

Tetrahedral coordination of ZnO is also an indicator of sp^3 covalent bonding. The Zn-O bonds possess a strong ionic character and thus ZnO lies on the borderline between covalent classification and ionic compound [8-12].

Except from the wurtzite phase, ZnO also crystallizes as cubic zincblend and rocksalt (NaCl) structures. Zincblend is known to be stable on cubic structure only by growth, while the rocksalt structure can not be epitaxially stabilized, because of its high-pressure metastable phase forming at around 10 GPa [13].

As stated above, Zinc oxide has an exciton with a binding energy of 60 meV. Excitons are basically weakly bound electron-hole pairs (Wannier Excitons). This binding occurs in semiconductors with low dielectric functions, where the shielding charges are relatively weak, so Coulomb potentials between negative charged electrons and positive holes are higher than their combined thermal energies [14]. Along with its high binding energy, an exciton in ZnO has a high luminescence efficiency making it primary candidate for a possible lasing material for a UV polariton laser [15]. By using above-gap photoexcitation it was observed that there is a two-step process in the exciton formation: the thermalization and cooling of the electron-hole plasma gas allows the formation of excitons with excess center of mass momentum (K≠0) and secondly a relaxation to the K = 0 occur. [16].

2.2 Stoichiometry or non and oxygen vacancies

2.2.1 Stoichiometry and non-stoichiometry

Generally most of the oxide materials are used as transparent conductors and are known to be n-type. The meaning of n-type is that its conductivity is due to the transport of electrons, while in p-type it is due to the transport of holes. High n-conductivity is observed in metal oxide which results from the anion deficiency that usually appears inside the crystal lattices in the form of oxygen vacancies.

Chemical formulas for binary oxides are usually written in a way to indicate that there is a definite ratio of cations to anions in the crystal, M_aO_b, where a and b are determined by the valency of the constituent atoms. When the material contain M and O atoms in the exact ratio *a/b*, then its composition is stoichiometric, though when a metal oxide is completely stoichiometric it is known as an ionic conductor whereas materials of this form can not be used as transparent conductors because of the high activation energy required for ionic conductivity. <u>Metal oxides used for transparent conductors are not completely stoichiometric.</u>

Non stoichiometry in metal oxides can be a result of two things:
1. Oxygen deficiency with respect to stoichiometric composition
2. Metal deficiency (or an excess of oxygen) with respect to stoichiometric composition

Inside a compound, non-stroichiometry equals to point defects in the crystal lattice compared to that in stroichiometric condition, while the extent of non-stoichiometry is also a measure of the net concentration of the corresponding type of defect in the compound. When a metal oxide is non-stoichiometric, oxygen deficient, dominant effects may be either oxygen vacancies or excess metal, or both type of defects. The way that oxygen vacancies are formed, lead to the formation of free electrons, thus oxygen deficient metal oxides are characterized by n-type conductivity. When a non-stoichiometric oxide is metal deficient, dominant defects may be metal vacancies, or interstitial oxygen atoms (excess of oxygen).The way metal defects are formed leads to the formation of positive electronic defect (holes), thus metal deficient metal oxides are characterized by p-type conductivity.

Regarding In_2O_3, oxygen deficiency is observed usually as oxygen vacancies acting as doubly charged doors giving electrons to the conduction band (in accordance with the 2/3 cation/anion ratio). If non-stoichiometric Indium Oxide contains an amount of x doubly charged oxygen vacancies, $V_o^{..}$, it is written as $In_2O_3(V_o^{..})e_{2x}$, but it can also be written as InO_x. Oxygen deficiencies in InO_x may be equivalent to the presence of excess indium compared to the stoichiometric composition **[17]**. This means, that the dominant defects are interstitial In^{+3} cations with a possible contribution to the conductivity of a maximum 0.1%, so their contribution is not taken account in the conductivity of the film.

In a perfect and pure single crystal (no point defects, no impurities), ZnO would be an insulator rather than a semiconductor at room temperature. The concentration of free electrons in the conduction band would amount only 4 m^{-3} compared to 10^{14}-10^{25} m^{-3} in most semiconductors. Real single ZnO crystals though exhibit n-type conductivity with an electron concentration varying over the whole range given for semiconductors, over more than 10 orders of magnitude. This large variation is caused mainly by its lattice non-stoichiometry and by donor impurities, which are located in the gap below the lower conduction band edge some 0.025-0.5 eV. Non-stoichiometry is due to native point defects like interstitial Zinc (Zn_i) or oxygen vacancies (V_0) which are generated thermally by variation of oxygen (or zinc) pressure and temperature [18].

2.2.2 Oxygen Vacancies

It is widely known that in a crystal (or an ionic compound) atoms are charged and the anions and cations are attributed with a definite valence. In oxides, oxygen ions are considered to have a valence of -2, cations have a positive valence, so the sum of positive and negative charges in the compound are equal to zero. The point defects that may exist in the compound are neutral or charged. If a crystal is to be electrically neutral then the sum of all effective positive charges must be equal with the sum of all effective negative charges.

The process of oxygen vacancies formation in a binary metal oxide is as follows: An oxygen vacancy is formed when an oxygen atom is removed. Two negative charges of the oxygen ion are left in the crystal. If both of these negative charges are localized at the oxygen vacancy, then the charge is the same as the charge in a perfect crystal. If that is the case, oxygen vacancies has zero effective charge. If the negative charges are electrons then if one or both of them are excited and transferred away from the vacancy, oxygen vacancy becomes singly or doubly ionized. As electrons are removed then the ionized oxygen vacancy will have a positive effective charge. This charged oxygen vacancy becomes an electron trapping site but in this process ore or two electrons are available for conduction [19]. A typical number for free electron concentration in binary oxides is in the region of 10^{17} – 10^{23} cm^{-3}. Oxides used as transparent conductors are all chemically unstable, thus they are easily oxidized and reduced. Based on this process; metal oxides are widely used as effective gas sensing elements and organic compounds [20,21].

3. EXPERIMENTAL TECHNIQUES AND METHODS USED FOR THE GROWTH AND CHARACTERIZATION OF IN$_2$O$_3$ AND ZnO FILMS

3.1 Sputtering deposition technique

3.1.1 Sputtering deposition process

Sputtering deposition is widely used in the development of Indium Oxide and Zinc Oxide, as thin films and other microelectronic applications. The process is simple, atoms or ions with energy of several keV bombard a solid surface, then single atoms (or molecules, clusters) will deposit on the surroundings. A dc and rf sputtering schematic can be seen in **Figure 3.1**.
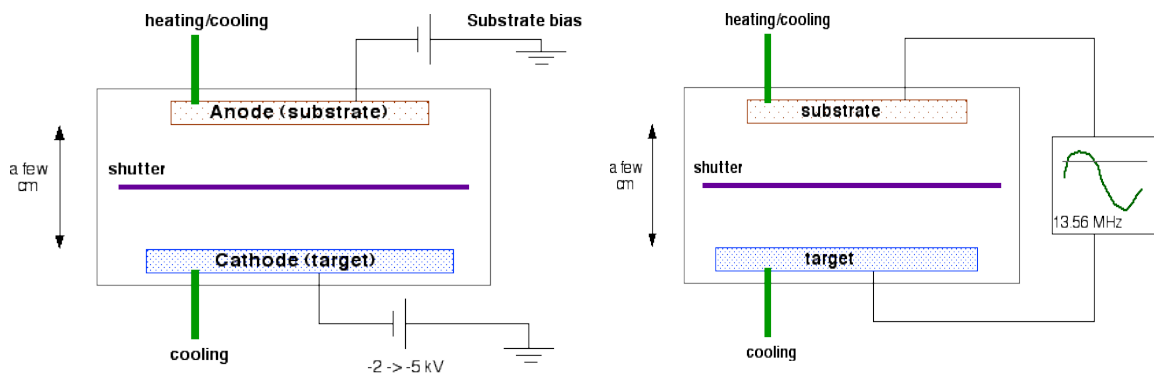
Fig. 3.1 *Schematic of a dc and of an rf sputtering system*

The target, also known as cathode because it is connected to the negative terminal, is a plate of the material to be deposited**.** The substrate, also known as the anode, may be grounded, but is always facing the target, biased positively or negatively, either cooled or heated, or with a combination of those. After creating vacuum inside the chamber, an inert gas, in most cases argon (in a pressure of 100 mTorr usually), is injected and is the medium in which a discharge is initiated and sustained. For the film to start growing in the substrate a visible glow discharge must be maintained between the electrodes. The process which the glow discharge progress is as follows: for starters, a small current flow in the chamber due to the small number of particles inside. As the voltage is increased, sufficient energy is imparted to the charged particles, thus more carriers are created (neutral atoms, positive ions and electrons). Electrons accelerate toward the anode by the electric field and produce additional ions by impact ionization. Positive ions strike the cathode transferring energy to the neutral atoms at the target surface. Some of the neutral atoms that acquire enough energy, are ejected from the target, and enter and pass through the discharge region and deposit on the film. Secondary electrons are emitted from the target and accelerate towards the anode producing new ions at the gas. When enough electrons are generated, they produce sufficient ions to regenerate the same number of initial electrons and thus sustain the discharge. The gas begins to glow and the voltage drops followed by a sharp increase in the current. Initially, ion bombardment of the cathode is not uniform but is concentrated near the cathode edges. While applying more power,

bombardment spreads over the whole cathode surface until a uniform current density is achieved. Further increase in power results in higher voltage and current density levels. The "abnormal discharge" state is entered and this is the operative region for sputtering **[22-25]**.

For the preparation of thin semiconducting films, the techniques used mainly, are sputtering and evaporation, mostly due to their low cost and the easiness of the process. However, sputtering process has the following over evaporation:
- Thickness control during the process
- Smoothness of surface of the film
- Good adhesion
- Good film uniformity
- Less waste of material

There are four sputtering techniques:
- dc
- rf
- magnetron
- reactive

There are a lot of variants within each technique, such as dc bias, and crossbreads between them, such as reactive dc, etc. In all the techniques, atoms are ejected from the target with the same mechanism, energy exchange between energetic particles and surface atoms. Magnetron sputtering allows higher deposition rates compared to conventional one. In reactive sputtering, films of compounds may be deposited on substrates from metallic targets in the presence of reactive gases mixed with the Argon (Ar, inert gas of deposition). By varying reactive gas pressure, deposition process is controlled and so is the composition of the film.
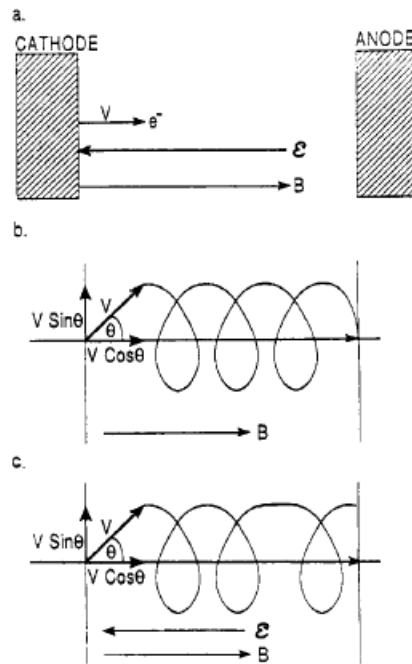
3.1.2 Magnetron sputtering

In our work, all samples were produced using dc magnetron sputtering. In this technique, only the electric field affects the electrons between the target and the substrate. When we impose magnet field (**B**), on the electric field (**E**) between target and substrate, electrons orbit in a different motion **[26]**. Electrons within this field experience a Lorentz force in addition to electric force:

$$F = m\frac{du}{dt} = -q(E + v \times B) \tag{3.1}$$

q is the electron charge, m is the mass and u the velocity. If the electric and the magnetic fields are parallel, secondary electrons are emitted exactly normal to the target surface and parallel to both fields, then the $v \times B$ equals to zero. If this is the case then, electrons are influenced only be the electric field, which accelerates towards the anode. If we neglect the electric field but the magnetic field is still applied, then if an electron is emitted from the cathode with u velocity at a θ angle in

respect to the magnetic field, then it experience a force of $qub\sin\theta$ in a direction perpendicular to B. As such, the electrons orbit in a circular motion with a radius r which is determined by the balance of the centrifugal force and the Lorentz force equal to $r = \frac{mu}{qB}\sin\theta$ and its motion is helical with a constant velocity of $u\cos\theta$. If the electron is emitted at an angle in respect to both the electric and the magnetic fields then its motion is more complex. It has a helical motion with a constant radius, but because of the electron acceleration, pitch of the helix increases. Result of this movement is a larger discharge current, thus a higher deposition rate.

Fig. 3.2. a.) *Linear motion when **E** is parallel to **B** (θ=0),* **b.)** *Helical orbit when **E**=0 and **B**≠0,* **c.)** *Helical orbit when **E** is parallel to **B** (θ≠0)*

In magnetron sputtering, the electron is trapped near the cathode, increasing the ionizing efficiency, resulting in much higher deposition rates. This is accomplished by employing a magnetic field parallel to the target and perpendicular to the electric field [27]. The magnetic lines come out normal to the target, then bend with a component parallel to the target surface and then return completing the magnetic circuit. As such, electrons emitted from the cathode are accelerated toward the anode, performing a helical action, but bent in an orbit back to the target when they reach the parallel magnetic field. The parametric equations, resulting from solving the differential equations from the 3 components of equation 3.1, are:

$$x = \frac{Et}{B}\left[1 - \frac{\sin(\omega_c t)}{\omega_c t}\right] \tag{3.2}$$

$$y = \frac{qE}{m\omega_c^2}[1 - \cos(\omega_c t)] \tag{3.3}$$

x and y are the distances along and above the target and $\omega_c = qB/m$. These equations are used to describe the cycloidal motion that the electrons perform within the cathode

space where electrical and magnetic fields are present. If electrons stay inside the negative glow region where the electric field is small, they perform a circular motion before collisions drive them back into the dark space or towards the anode.

3.1.3 DC Sputtering Equipment

The sputtering equipment used for the deposition of Indium Oxide and Zinc Oxide films is a dc planar reactive magnetron sputtering from ALCATEL and can be seen in **Fig. 3.3 [28]**.
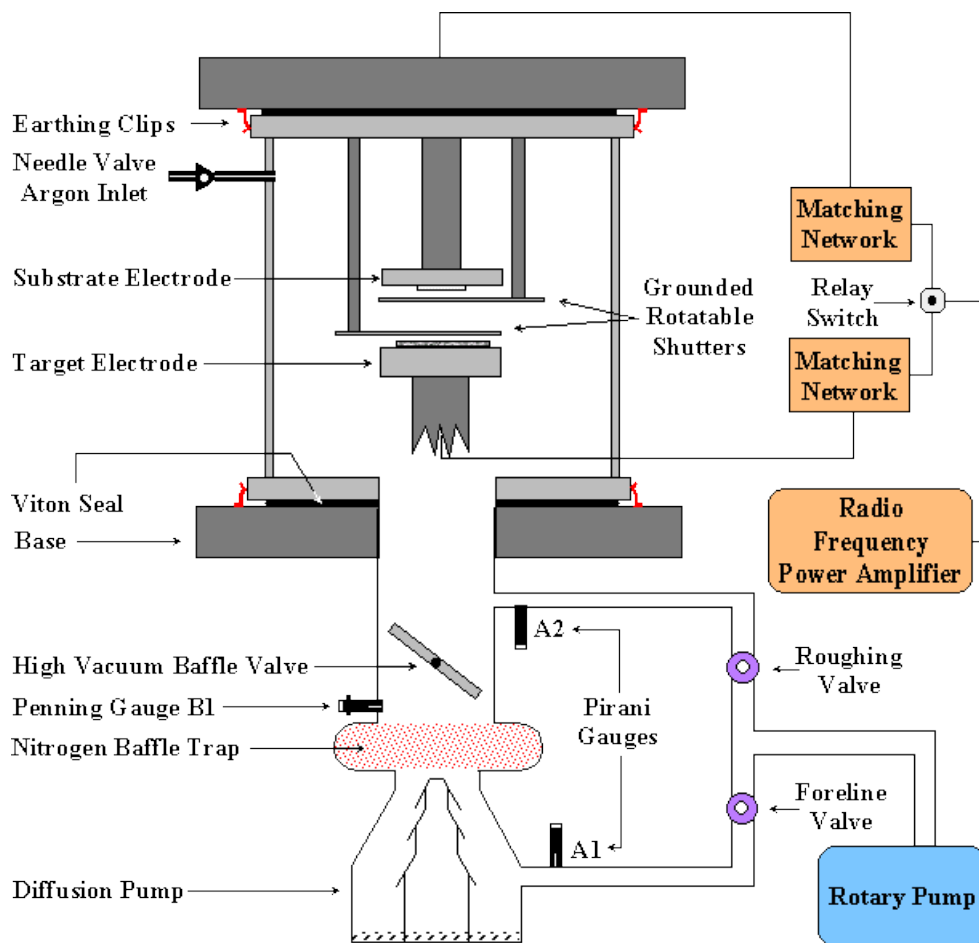

Fig. 3.3 Dc sputtering equipment

The equipment consists of a vacuum chamber; it is the area where the deposition process takes place, a pumping system, a gas supply system and a power supply system. Deposition system is of cylindrical shape with a square base of 0.28 m^2 and a height of 0.4 m and it is made of stainless steel. It also consists of two plane circular sputter sources (Targets) with 15 cm diameter each. It has permanent magnets placed at the back of the targets in a suitable arrangement for the production of the magnetic field. The targets are cooled by water circulation during the sputtering process. Above the sputter sources at a distance of 6 cm and parallel to them, a substrate holder is placed with the availability to be rotated. On the substrate holder, plane circular sample holders with a diameter of 9 cm are placed and can be transferred outside of

the chamber so it can be easier to place or exchange the samples on it. This system forms the substrate for the deposited material. On the substrate holder, we can place 4 samples with dimensions of 1.5 cm × 1.5 cm each for every deposition run. Substrate holder is also cooled at room temperature by the water circulation system during the deposition.

Vacuum pumping system consists of a rotary mechanical pump, used for pre-pumping, and an oil diffusion pump, used to achieve high vacuum. To achieve even higher vacuum, a liquid nitrogen pump is adjusted to the pumping system. Using this equipment, chamber is evacuated primarily to a base pressure of 10^{-7} mbar. After achieving this pressure, introduction of the gases can begin, (Argon, as sputtering gas and Oxygen as the reactive gas, in our depositions) and can be controlled by mass flow controllers. The pressure of the chamber is measured by two manometers (pressure gauges) which cover different values of pressure. The Pirani type is used for measuring pressures in the region of atmospheric pressure to 10^{-4} mbar, whereas for lower pressures (till 10^{-7}), the Penning type is used. Dc voltage is provided by a dc power supply unit and is applied to the targets using a selector, while the dc voltage and current can be controlled independently.

3.2 Optical properties of semiconducting thin films, methods and techniques used for characterization

3.2.1. Introduction

Optical characterization is the process which allows the investigation of the optical properties, the energy band gap and the film thickness. In the present work we used an A-step, an UV-VIS spectrometer and a theoretical method with the use of equations toped with spectroscopic ellipsometry.

3.2.2. Optical constants

The optical constants of thin films are necessary to be calculated so to evaluate the optical properties of transparent semiconducting films. Optical properties rely in the different angle of propagation of electromagnetic radiation in materials compared to that in free space because of the presence of charge, resulting in a change of the wave of velocity and intensity of the radiation, described by the complex index of refraction:

$$n_c \equiv n - ik \tag{3.4}$$

whereas n is the refractive index of the material and k is the absorption index, also known as extinction coefficient.

Light can be absorbed, reflected or scattered when it 'hits' the surface of the material. Absorption by bound charges or charge carrier and molecular scattering can result in loss of light. Same type of absorption can also occur in the substrate of the thin films and the effect of this is subtracted from the data. Reflection occurs at the point where two matters come in touch, air-thin film, thin film-substrate and substrate-air.

Ratio of the transmitted light intensity I to the incident light intensity I_0, when light pass through absorbing film is given by Lambert's law equation:

$$I = I_0 e^{-ad} \tag{3.5}$$

a is the absorption coefficient and d is the thickness of the film. Absorption coefficient relates to extinction coefficient k through the equation:

$$a = \frac{4\pi k}{\lambda} \tag{3.6}$$

λ is the wavelength of light.

3.2.3. Determination of refractive index and thickness of a transparent film on a transparent substrate, using equations

In our experimental work we used as transparent substrates corning glass, along with PEN (polyethylene naphthalate), PET (polyethylene-terephthalate) and quartz substratess. Substrate and thin film surfaces were smooth. In this section, theory of the optical behavior of thin films will be presented. Transmission T and reflectance R depend on the refractive index n_1 and thickness d of the film, wavelength λ of the light and the refractive index of the substrate n_2.
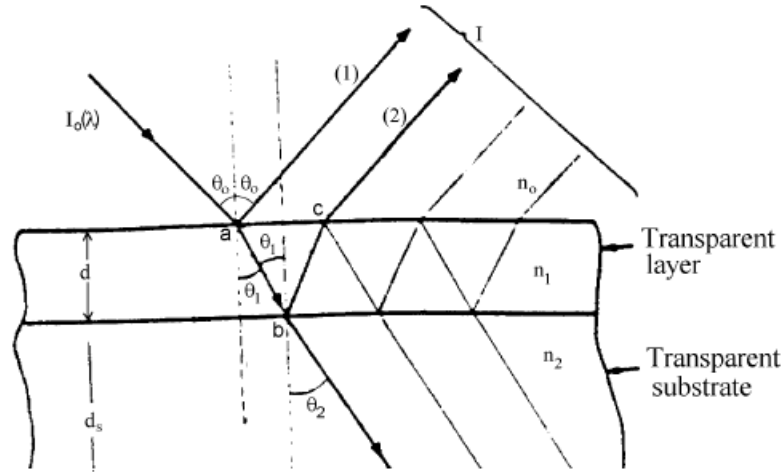
Fig. 3.4. *System of air-thin film-substrate. Transmission and reflection of light by a thin film* **[25]**

Our substrate thickness d_s is in the region of 0.4 mm (corning glass) and is much larger than the thickness of the thin film d (normally less than 1μm). Angle of incidence in our system is θ_0. Incident ray is partly reflected back to the surface of the film and partly transmitted at an angle θ_1. Upon reaching the interface thin film-substrate, the transmitted part of light is partly reflected to the surface of the film and party transmitted at an angle θ_2. These three angles θ_0, θ_1 and θ_2 can be calculated by Snell's law: $n_0 sin\theta_0 = n_1 sin\theta_1 = n_2 sin\theta_2$

The optical pathlength of rays is calculated through the equation **[29]**:

$$\Delta = 2n_1 d cos\theta_1 \tag{3.7}$$

Reflectance and transmittance are calculated by the summation of the multiple reflected and transmitted beams, measuring first the phase difference δ between the beams:

$$\delta = \left(\frac{\Delta}{\lambda}\right)\pi = \frac{2\pi}{\lambda}n_1 d cos\theta_1 \tag{3.8}$$

Consequently, the result of the summation for the reflected and transmitted amplitude:

$$A = \frac{r_1 + r_2 \exp(-2i\delta)}{1 + r_1 r_2 \exp(-2i\delta)} \tag{3.9}$$

$$B = \frac{t_1 t_2 \exp(-i\delta)}{1 + r_1 r_2 \exp(-2i\delta)} \tag{3.10}$$

and having calculated the summations, reflectance and transmittance can be found using the following equations:

$$R = \frac{r_1^2 + 2r_1 r_2 \cos 2\delta + r_2^2}{1 + 2r_1 r_2 \cos 2\delta + r_1^2 r_2^2} \tag{3.11}$$

$$T = \frac{n_2}{n_0} \cdot \frac{t_1^2 t_2^2}{1 + 2r_1 r_2 \cos 2\delta + r_1^2 r_2^2} \tag{3.12}$$

where r and t represent the Fresnel coefficients of reflectance and transmittance and depend on the polarization of the incident light. If the polarization is in the plane of the incidence, then the Fresnel coefficients with the help of Snell's law can be calculated as follows:

$$r_1 = r_{1_p} = \frac{\tan(\theta_1 - \theta_0)}{\tan(\theta_1 + \theta_0)} \qquad r_2 = r_{2_p} = \frac{\tan(\theta_2 - \theta_1)}{\tan(\theta_2 + \theta_1)} \tag{3.13}$$

$$t_1 = t_{1_p} = \frac{2\sin\theta_1 \cos\theta_0}{\sin(\theta_1 + \theta_0)\cos(\theta_1 - \theta_0)} \qquad t_2 = t_{2_p} = \frac{2\sin\theta_2 \cos\theta_1}{\sin(\theta_2 + \theta_1)\cos(\theta_2 - \theta_1)} \tag{3.14}$$

If the polarization is normal then they take the form:

$$r_1 = r_{1_p} = \frac{\sin(\theta_1 - \theta_0)}{\sin(\theta_1 + \theta_0)} \qquad r_2 = r_{2_p} = \frac{\sin(\theta_2 - \theta_1)}{\sin(\theta_2 + \theta_1)} \tag{3.15}$$

$$t_1 = t_{1_p} = \frac{2\sin\theta_1 \cos\theta_0}{\sin(\theta_1 + \theta_0)} \qquad t_2 = t_{2_p} = \frac{2\sin\theta_2 \cos\theta_1}{\sin(\theta_2 + \theta_1)} \tag{3.16}$$

If the surrounding media is absorbing, the values of the refractive indexes are replaced by the complex refractive index n_c.

In this work, for the determination of optical constants and thickness of our thin films we used the equations first introduced by Manifacier *et al.* **[30,31]**. It is a straightforward procedure to deduce the optical constants and thickness by using the fringe pattern of the transmission spectrum of the thin film surrounded by non-absorbing media. In our case, the film with a complex refractive index n_1, is bounded by two media, also transparent, with refractive indexes of n_0 and n_2 for the case of normal incidence.

According to equation (3.10), the amplitude of the transmitted beam is:

$$B = \frac{t_1 t_2 \exp(-2\pi n_1 {}^d/_\lambda)}{1 + r_1 r_2 \exp(4\pi n_1 {}^d/_\lambda)} \tag{3.17}$$

Where r_1, r_2 are the reflection coefficients and t_1, t_2 are the transmission coefficients, calculated by equations (3.15) and (3.16).

Transmission can be calculated now by equation (3.12):

$$T = \frac{n_2}{n_0}|B|^2 = \frac{16n_0n_2(n^2+k^2)b}{A'+B'b^2+2b\left[C'\cos\left(4\pi nd/\lambda\right)+D'\sin\left(4\pi nd/\lambda\right)\right]} \tag{3.18}$$

Where for normal absorption: $A' = [(n+n_0)^2 + k^2][(n+n_2)^2 + k^2]$

$B' = [(n-n_0)^2 + k^2][(n-n_2)^2 + k^2]$

$C' = -(n^2 - n_0^2 + k^2)(n^2 - n_2^2 + k^2) + 4k^2 n_0 n_2$

$D' = 2kn_2(n^2 - n_0^2 + k^2) + 2kn_0(n^2 - n_2^2 + k^2)$

$$b = \exp\left(-4\pi kd/\lambda\right) = \exp(-ad) \tag{3.19}$$

$$a = 4\pi k/\lambda$$

with a been the absorption coefficient.

In the case of weak absorption, $k^2 \ll n^2$, $k^2 \ll (n-n_0)^2$ and $k^2 \ll (n-n_2)^2$, we get:

$A' = (n+n_0)^2(n+n_2)^2 \equiv C_1^2,$

$B' = (n-n_0)^2(n_2-n)^2 \equiv C_2^2,$

$C' = -(n^2 - n_0^2)(n^2 - n_2^2) = C_1 C_2$

where for $D' \ll C'$ the term $D'\sin(4\pi nd/\lambda)$ is neglected. As such, transmittance in weak absorption is written as:

$$T = \frac{16n_0n_2n^2b}{C_1^2+C_2^2b^2+2C_1C_2b\cos\left(4\pi nd/\lambda\right)} \tag{3.20}$$

In both transmittance and reflectance spectrum, we observe that they exhibit interference fringes (shown as oscillations) versus wavelength in wavelength regions outside the fundamental absorption (E_G, energy band gap of the film) or the free carrier absorption, where film is transparent. Interference fringes appear as maxima and minima T in the transmission spectrum and occur for:

$$\frac{4\pi nd}{\lambda} = m\pi \tag{3.21}$$

where m is the order of interference fringes in the transmission spectrum. This equation is used for the production of interference fringes.

Transmission maxima and minima values are given by:

$$T_{max} = \frac{16n_0n_2n^2b}{(C_1-C_2b)^2} \tag{3.22}$$

$$T_{min} = \frac{16 n_0 n_2 n^2 b}{(C_1 + C_2 b)^2} \qquad (3.23)$$

Manifacier *et al.* consider T_{max} and T_{min} as continuous functions of λ. These functions are the envelopes of maxima and minima in the transmission spectrum as can be seen in **Figure 3.5**.
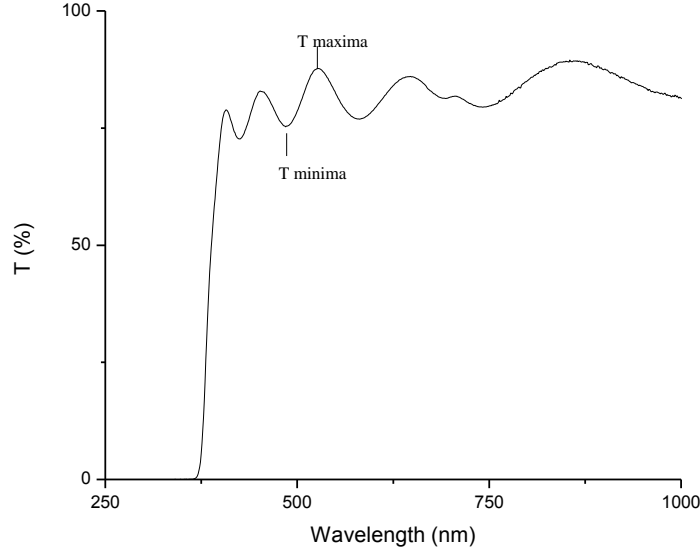
Fig. 3.5 Transmission spectrum for ZnO film of thickness in the region of 750 nm.

Then the ratio of the equations (3.22) and (3.23) gives:

$$b = \frac{C_1 \left[1 - (T_{max}/T_{min})^{1/2} \right]}{C_2 \left[1 + (T_{max}/T_{min})^{1/2} \right]} \qquad (3.24)$$

By substituting this ratio into the equation for maxima one gets the refractive index (n):

$$n = \left[N + (N^2 - n_0^2 n_2^2)^{1/2} \right]^{1/2} \qquad (3.25)$$

Where $N = \frac{n_0^2 + n_2^2}{2} + 2 n_0 n_2 \frac{T_{max} - T_{min}}{T_{max} \, T_{min}}$

Thus the refractive index n is determined by transmission maxima and minima at the same wavelength, provided the values of refractive index of air and substrate are known. Knowing the refractive index of our thin films, we can calculate the values of C_1 and C_2 and the ratio of maxima and minima. Then the thickness can be calculated from two maxima or two minima, from:

$$d = \frac{M_{12} \lambda_1 \lambda_2}{2 n (\lambda_1 - \lambda_2)} \qquad (3.26)$$

λ_1 and λ_2 are the wavelengths of the two extrema and M_{12} is the number of fringes separating those two extremas (for two adjacent maxima or minima

then the value of M_{12} is 1, and if we choose maxima and the adjacent minima then the value is ½). Knowing b and the thickness d, we can determine the extinction coefficient k and the absorption coefficient a from equation (3.19).

3.2.4   Fundamental absorption and optical gap determination

Initially an outline on the energy gap and fundamental absorption will be presented, before applying them to our work (InO_x and ZnO).

Fundamental absorption is related mostly to the excitation of an electron from valence band to conduction, i.e is a band to band transition, and as such can be used to determine the semiconductor energy gap. It is known, that the kinetic energy of the electron is written as:

$$E = \frac{p^2}{2m_e}$$
(3.27)

p is the crystal momentum and m_e is the effective mass of the electron. In quantum mechanics the crystal momentum is written as:

$$p = \hbar k$$
(3.28)

where k is the wave vector, in the case of semiconductors the "the momentum vector". Thus the kinetic energy can be rewritten as:

$$E = \frac{\hbar^2 k^2}{2m_e}$$
(3.29)

For holes, the only difference is that we use their effective mass m_h. Photon absorption process is described by the absorption coefficient a(hv), which for a given photon energy is proportional to the probability (P_{if}) of the transition, from an initial (i) state to the final (f) state, and the density of electrons in the initial n_i state and the density of the empty (available) final state n_f:

$$a(hv) = A \sum P_{if} n_i n_f$$
(3.30)

It is assumed that all the lower states are filled and all the upper states are empty. The dependence of the absorption coefficient a with photon energy hv is different for direct transitions and indirect ones. However, since both In_2O_3 and ZnO are semiconductors with direct transitions, we will present their transitions only (**Figure 3.6)**
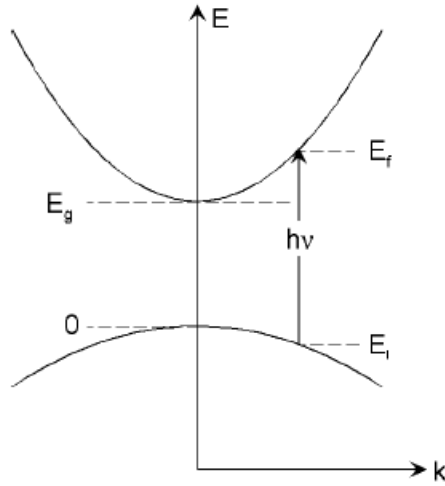
Fig. 3.6 Schematic of a direct absorption transmission [29]

For transitions between two direct valleys at crystal momentum k = 0, transition probability is independent of photon energy and therefore can be taken as a constant. The initial energy state can be associated with the final energy state as:

$$E_f = hv - |E_i|$$ (3.31)

For parabolic bands:

$$E_f - E_g = \frac{\hbar^2 k^2}{2m_e} \qquad \text{and} \qquad E_i = \frac{\hbar^2 k^2}{2m_h}$$ (3.32)

So: $hv - E_g = \dfrac{\hbar^2 k^2}{2}\left(\dfrac{1}{m_e} + \dfrac{1}{m_h}\right)$ (3.33)

$\left(\dfrac{1}{m_e} + \dfrac{1}{m_h}\right) = \dfrac{1}{m_r}$, and m_r is the reduced mass.

The density of directly associated states can be written as [32]:

$$N(hv)d(hv) = \frac{8\pi k^2 dk}{(2\pi)^3} = \frac{(2m_3)^{\frac{3}{2}}}{2\pi^2 \hbar^3}\left(hv - E_g\right)^{\frac{1}{2}}d(hv)$$ (3.34)

Using equations (3.30) and (3.34), one gets:

$$a(hv) = A^*(hv - E_g)^{1/2}$$ (3.35)

When *a* is equivalent to zero, then the value of E_g is equivalent to *hv* (h is also expressed in eV).

In the case of heavily doped semiconductor, then the Fermi level is inside the conduction band (for n-type material), or inside the valence banc (for p-type material) by a quantity of ξ. For a n-type material this can be seen in **Figure 3.7**.
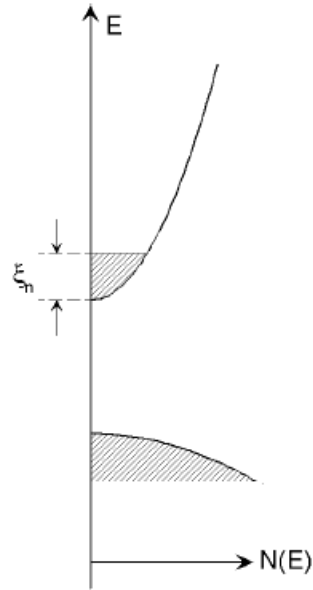
Fig. 3.7 *n-type energy/density of states diagram, for heavily doped material [29]*

According to **Fig 3.7**, states below ξ_n are filled, so fundamental transitions to states below the point with energy $E_g + \xi_n$ are forbidden. Therefore, the absorption edge should lift to higher energies by about ξ_n. This shift of the absorption band is also known as Burstein-Moss shift **[33, 34]**. Then the energy shift is calculated by:

$$E_g - E_{g_0} = \frac{\pi^2 h^2}{2m} \left(\frac{3n_e}{\pi}\right)^{3/2} \qquad (3.36)$$

E_{g_0} is the intrinsic band gap and m is the effective mass.

3.2.5 Stylus profilometer

Thickness of the deposited films is also measured by use of a stylus profilometer. Stylus method consists of measuring the mechanical movement of a stylus as it traces the topography of the film-substrate step. A diamond needle stylus serves as the electromagnetic pickup. Stylus force is adjustable from 1 to 30mg and vertical magnifications of a few thousands up to a million times are possible. Thickness is directly read out as the height of the step-contour trace.

3.3 Spectroscopic Ellipsometry

3.3.1 Introduction and History

Ellipsometry was first developed by Drude in 1887. He also derived the equations of ellipsometry also known as 'the Drude model' which expresses the optical properties of metals. Until the early 1970's ellipsometry was operated manually. In 1975, Aspnes *et al.* [35] realized the complete automation of spectroscopic ellipsometry measurements. The first real time monitoring ellipsometer was developed by Muller and Farmer [36], increasing the number of measurement data. In 1990, a group of researchers from the Pennsylvania State University developed a real time instrument, which is used widely until now, with a photodiode array detector, allowing measurements of light intensities at different multiwavelengths in the same time [37]. Due to the rapid development in computer technology, spectroscopic ellipsometry developed rapidly, expanding its application field. Spectroscopic ellipsometry allows for an in situ analysis (real time) of the samples used by employing light as a measurement probe.

3.3.2 Features of Spectroscopic Ellipsometry

Ellipsometry is an optical measurement technique based on light transmission or reflection from samples [38-40]. Ellipsometry studies the fact that polarized light often becomes 'elliptical' upon light reflection. Key feature is the measurement of the change in polarized light upon light reflection on a sample (in our work metal oxide semiconducting thin films). Ellipsometry measures two values: amplitude ratio ψ and phase difference Δ between light waves known as p- and s- polarized light waves. Spectra are subject to changes in the wavelength of light. The study is carried out in the ultraviolet/visible region, but can also be performed in the infrared region.

In real-time monitoring, except for characterization of thin film thickness, etching and thermal oxidation can be performed. Spectroscopic ellipsometry allows also the characterization of thin films formed by a solution, as light is employed as probe. However, there are two restrictions on the measurements:

1) The surface roughness of the thin films has to be small,
2) Measurements must be performed at oblique incidence.

If light intensity is severely reduced due to surface roughness, measurements are less as ellipsometry determines a polarization state from its light intensity. If roughness exceeds ~30%, errors in the measurements generally increase.

In spectroscopic ellipsometry, incidence angle is chosen so that the sensitivity of the measurement is maximized. The choice, though, of the angle varies according to the optical constants of the sample. For our samples we used incidence angles

near the Brewster angle, 65°-70°-75°. Ellipsometry measurements cannot be performed at normal incidence, due to the fact that p- and s- polarizations cannot be distinguished at this angle.

By using spectroscopic ellipsometry for measurements on our samples we had the following advantages:

a. High precision measurements
b. Very high thickness sensitivity, ~0.1 Å
c. Fast and non-destructive measurement
d. Wide series of characterizations such as optical constant and film thickness measurement

Even though this technique provides us with those advantages, characterization of our samples using spectroscopic ellipsometry had some disadvantages, such as:

a. Necessity of an optical model in data analysis
b. Complicated analysis
c. Low spatial resolution
d. Characterization of low absorption coefficients is difficult, $a < 100$ cm^{-1}

Spot size of the light beam used is several millimeters, making possible the determination of the surface area ratio of the materials that covers the thin film.

3.3.5 Ellipsometric Configurations

The basic configuration of an ellipsometer (described best at H.G. Tompkins and E.A. Irene [41]) can be seen in **Figure 3.8**.
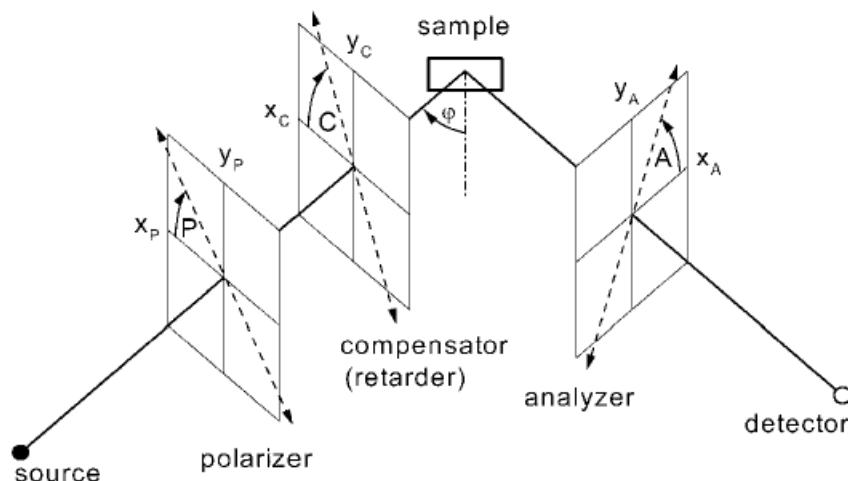

Fig. 3.8 Schematic configuration of an ellipsometer [37]

It consists of a light source, a linear polarizer (P), compensator C, sample (S), analyzer (a) and a detector. The triangle source-polarizer-retarder is known as polarization state of light incident on the sample. The system analyzer-detector is

used to detect the change of polarization produced by the sample. The beam, incident on and reflected from the sample, lie in the plane of incidence, which contains the normal to the sample surface. Oblique incidence ($\varphi>0$) is typical, since it leads to pronounced changes of the polarization. The reason is a pronounced difference in the behavior of the two basic linear polarizations, the one parallel to the plane of incidence, known as p-polarization, and perpendicular to it, s-polarization.

3.3.4 Data Analysis

An optical model represented by the complex refractive index of air (N_0), thin film (N_1) and substrate, as can be seen in **Figure 3.9**.
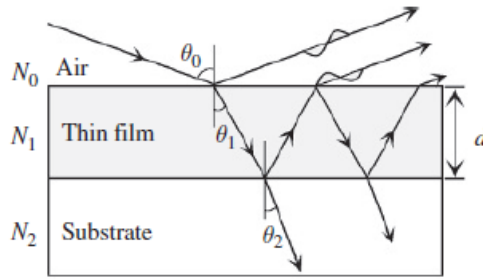
Fig. 3.9 Optical model with Air/thin film/substrate structure

In ellipsometry, the two parameters (ψ, Δ) are defined by ρ = $\tan\psi\exp(i\Delta)$. ρ is expressed also by the following equation:

$$tan\psi \exp(i\Delta) = \rho(N_o, N_1, N_2, d, \theta_0) \qquad (3.37)$$

In the data analysis, the dielectric function is required, $\varepsilon=\varepsilon_1-\iota\varepsilon_2$. When it is not known, then modeling is required. There are many dielectric function models and we select one according to the optical properties of our sample. Some of the models used are: for dielectric functions in a transparent region ($\varepsilon_2 \sim 0$), Sellmeier or Cauchy model is selected. For free-carrier absorption, Drude model is used. For electric polarization in the Ultra-Violet/Visible region we use the Lorentz or Tauc-Lorentz model.

For our work the Sellmeier-Cauchy model was selected: Complex refractive index of air is $N_0 = 1$ and the values of N_2 and θ_0 must be known in advance. In the (ψ, Δ) spectra there is an optical interference effect in the energy region, where absorption of light is small. Analysis of this pattern is used to estimate the thin film thickness d. With the thickness known, the only parameter need to be measured is the complex refractive index of the thin film N_1 and its parameters n_1 and k_1. These two values can be obtained directly from the (ψ, Δ) values. Supposing the dielectric function of the thin film changes smoothly in the region from E_n = initial to final, and the dielectric function is expressed from Cauchy model:

$$n = A + \frac{B}{\lambda^2} + \frac{C}{\lambda^4} + \cdots \qquad (3.38)$$

$$k = Dexp\big[(En - E_g)/E_u\big] \tag{3.39}$$

In this case, fitting from E_n = initial to final can be performed easily using the thickness d and the (A, B, C) parameters of Cauchy. As thickness d can be found from the analysis fitting, solving the equation (3.37) we convert the known (ψ, Δ) into

(n_1, k_1). This procedure is called mathematical inversion and is performed by using linear regression analysis. Thus, mathematical inversion is called optical constant fit and is used to calculate the optical constants of the whole measured range. This data analysis is quite effective in determining the dielectric function of our thin film, even in regions when determining it is difficult. Equation 3.39 shows the light absorption by the Urbach tail **[42, 43]**. Urbach tail is generated by the imperfection of semiconductor crystals, and the light absorption by the tail state near E_g is described by the Urbach energy E_u. In rare cases, it is utilized to express optical transitions that have no direct relation to the Urbach tail.

In the high-energy region, light absorption increases and the penetration depth tends to zero, thus optical interference is negligible in this region. Concluding, in spectroscopic ellipsometry, the study of (ψ, Δ) spectrum, provides characterization, in a wide energy range, of various physical properties.

As it is known, ε_1 and ε_2 are not independent of each other and if one of them varies, then the other one changes too. To describe the relation between them, the Kramers-Kronig relation is used:

$$\varepsilon_1(\omega) = 1 + \frac{2}{\pi} P \int_0^\infty \frac{\omega' \varepsilon_2(\omega')}{\omega'^2 - \omega^2} d\omega'$$

$$\varepsilon_2(\omega) = -\frac{2\omega}{\pi} P \int_0^\infty \frac{\varepsilon_1(\omega') - 1}{\omega'^2 - \omega^2} d\omega'$$

When ε_2 is known in the region from $\omega=0$ to ∞, then ε_1 can be estimated directly. Kramers-Kronig relations follow causality, meaning that light absorption occurs after light enters media. The Lorentz, Tauc-Lorentz and Drude models satisfies the conditions of Kramers-Kronig relation. The Sellmeier and Cauchy models, however, do not satisfy those conditions since in these models the ε_1 is obtained by assuming that ε_2 is non-existant.

So in few words the procedure of data analysis is:

1. Construction of an optical model
2. Selection or modeling of dielectric function
3. Fitting to (ψ, Δ) spectrum
4. Calculation of fitting error
5. Determination of optical constants and thickness
6. Judgment of result

For the calculation of fitting error, the following equation is used:

$$\sigma^2 = \frac{\Sigma[\rho_{ex}(h\nu_i) - \rho_{cal}(h\nu_i)]^2}{M-P-1},$$

M is the number of data points and P the number of parameters.

4. EXPERIMENTAL RESULTS AND DISCUSSION

4.1 Preparation of the films

In this work, our films have been deposited by a dc planar reactive magnetron sputtering of ALCATEL, in a mixture of argon-oxygen plasma, using a 99.999% pure Indium and Zinc target, in a total pressure of 8×10^{-3} mbar. Prior to deposition the pressure inside the vacuum chamber was 1×10^{-7}. Films used for the determination of thickness and energy band gap were in the region of 600-1600 nm, while for spectroscopic ellipsometry measurements, thicknesses were in the region of 200-550 nm. Before the main deposition, films target was presputtered for about 15 minutes to eliminate any differential sputtering effects and remove any contaminants that have been there from previous depositions.

In the present work, films were deposited onto Corning 1707F low alkali glass substrates (thickness of 0.4 mm), which had thermally evaporated NiCr electrodes used for conductivity measurements.

The preparation for the films used for spectroscopic measurements is presented:
Firstly we use ethanol on the back side of the corning glass. We mildly-roughen the back surface of the corning glass in order to avoid reflection/back-scattering. After finishing this procedure, we place our film into a peaker filled with acetone. Then, the film was placed for an ultrasonic bath for 15 minutes. We repeat the same procedure (15 minutes), replacing acetone with isopropanol. After the ultrasonic bath is finished, we cleaned the thin films with distilled water and had them dried by using nitrogen gas.

4.2 Optical properties

4.2.1 Transmission measurements and thickness calculation

Optical transmittance of our films was measured using a Perkin-Elmer UV/Vis transmission spectrometer; region of the wavelengths measured was from 200 nm (Uv region) to 1000 nm (Near Infrared region). Theoretical thicknesses of the films used for this part were in the region between 500 nm to 2000 nm (2 μm). In the transmission spectrum, as stated, we use the maxima or minima of the fringes that we have, to determine the thickness. To calculate though the thickness, first we had to calculate the refractive index of the thin film.

Refractive index n was calculated for all the samples by using the interference minima in their transmission spectrum. Condition for interference fringes is given by the equation (3.21):

$$\frac{4\pi nd}{\lambda} = m\pi,$$

m is the order of the fringe at a wavelength λ, n is the refractive index and d the measured thickness. If m is an even integer, it provides the interference maxima, while if m is an odd integer, it provides the interference minima. As such the conditions can be stated as:

$$4nd = m\lambda \tag{4.1}$$

$$4nd = (2m + 1)\lambda \tag{4.2}$$

The method used in the measurement of the films has been discussed in section 3.2.3. The complex refractive index of a transparent dielectric film is given by equation (3.4):

$$n_c = n - ik, \ k^2 \ll n^2$$

Where n is the refractive index, whereas k is the extinction coefficient. The refractive index n is calculated by equation (3.25):

$$n = \left[N + (N^2 - n_0^2 n_2^2)^{1/2}\right]^{1/2} \tag{4.3}$$

where: $N = \frac{n_0^2 + n_2^2}{2} + 2n_0 n_2 \frac{T_{max} - T_{min}}{T_{max} \ T_{min}}$ $\qquad$ (4.4)

Where n_0 is the refractive index of air and its value is 1, n_2 is the refractive index of glass; in our work corning glass has the same refractive index with glass, with value a of 1.5. T_{max} and T_{min}, are the maxima and minima measured at the same wavelength λ.

Knowing both the refractive index and the thickness of the film, we can calculate the extinction coefficient by using equations (3.19) and (3.24):
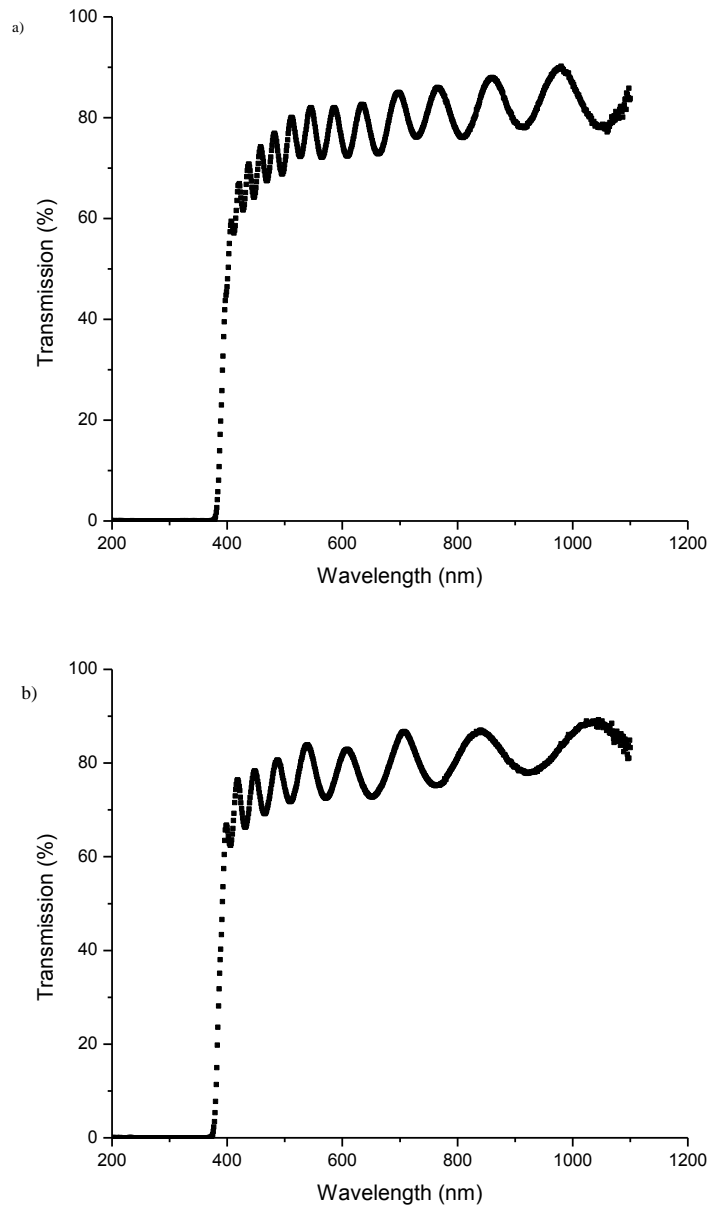
$$b = exp(-4\pi kd/\lambda) \text{ and} \tag{4.5}$$

$$b = \frac{C_1}{C_2} \frac{\left[1-(T_{max}\,/t_{min}\,)^{1/2}\right]}{\left[1+(T_{max}\,/t_{min}\,)^{1/2}\right]}$$

And $C_1 = (n+n_0)(n+n_2)$, $C_2 = (n-n_0)(n_2-n)$.

Thickness of the film is then calculated by using equation (3.26):

$$d = \frac{\lambda_1\lambda_2}{2n(\lambda_1-\lambda_2)}$$

The determination of the refractive index and thickness of our films was based on the transmission spectra seen in **Figure. 4.1** and **Figure. 4.2**.

Fig. 4.1 *Transmission spectrum of thin film with thickness: a) 1600 nm (1.6μm),*
b) 1000 nm (1 μm)

As observed, thin films with large thicknesses have many fringes. By having more fringes in the transmission spectrum, determination of the thickness is more precise, as there are more maxima and minima to integrate minimizing the risk for errors in the calculations.

For thin films with thickness lower than 1 μm, transmission spectrum has fewer fringes, making the determination of the thickness easier but with a high possibility of making the wrong calculation for the thickness.
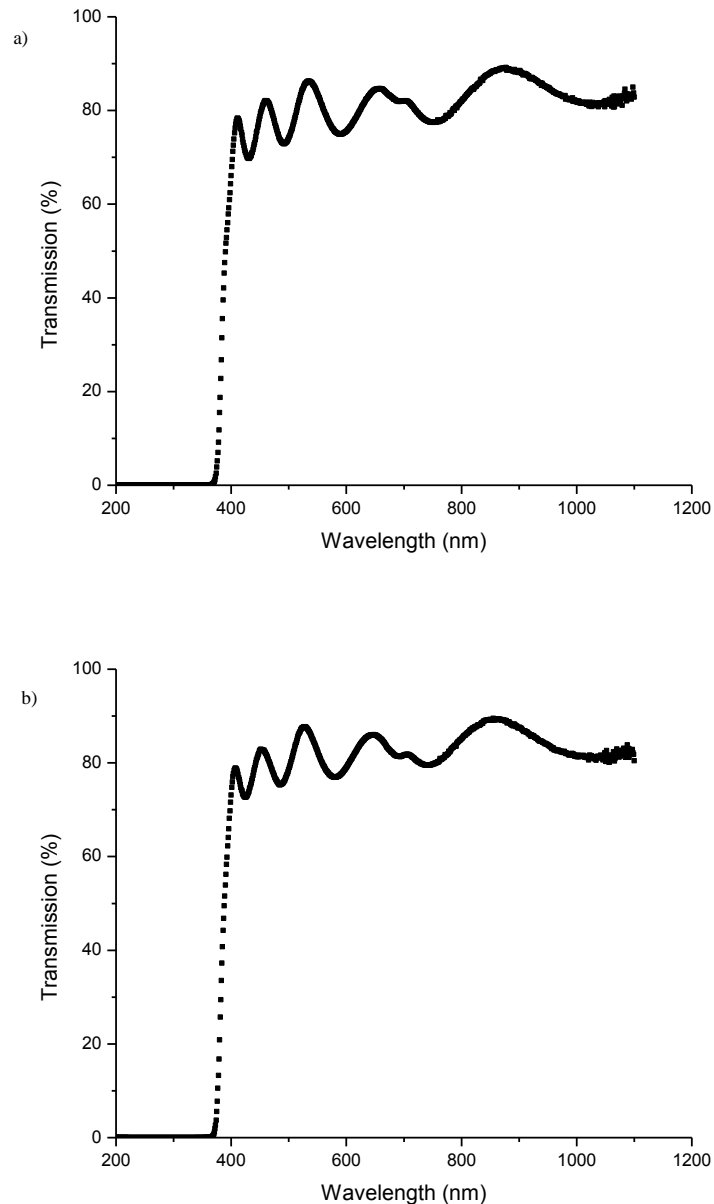
Fig. 4.2 *Transmission spectrum for thin films with thickness: a) 550 nm*
b) 650 nm

Before using equations (4.3) and (4.4) we determine the refractive index. For our samples, calculated values for n and k are presented in Tables **4.1, 4.2, 4.3, 4.4**:

Table 4.1: Optical constants for sample #420 (1600 nm)

λ (nm)	T min	T max	N	n
411.97	0.57	0.67	2.13	1.91
427.99	0.62	0.68	2.14	1.91
447.04	0.64	0.69	2.15	1.92
468.92	0.67	0.71	2.11	1.89
493.97	0.69	0.73	2.16	1.92
526.92	0.72	0.75	2.07	1.87
564.03	0.72	0.78	2.12	1.91
608.92	0.72	0.81	2.13	1.92

Table 4.2: Optical constants for sample #570 (1012 nm)

λ (nm)	T min	T max	N	n
401.93	0.57	0.67	2.42	2.08
427.99	0.62	0.74	2.40	2.07
460.98	0.65	0.77	2.31	2.02
504.99	0.68	0.80	2.28	2.00
567.92	0.70	0.82	2.23	1.97
643.99	0.71	0.83	2.25	1.98

Table 4.3: Optical constants for sample #626 (600 nm)

λ (nm)	T min	T max	N	n
424.01	0.73	0.81	2.04	1.85
484.95	0.75	0.85	2.10	1.89
581.05	0.76	0.87	2.07	1.87

Table 4.4: Optical constants for sample #507 (600 nm)

λ (nm)	T min	T max	N	n
430.97	0.69	0.80	2.19	1.94
491.98	0.73	0.84	2.18	1.93
558.97	0.75	0.85	2.11	1.90

In **Figure 4.3** we plot refractive index versus wavelength for our samples (#420, #570, #626, #507.
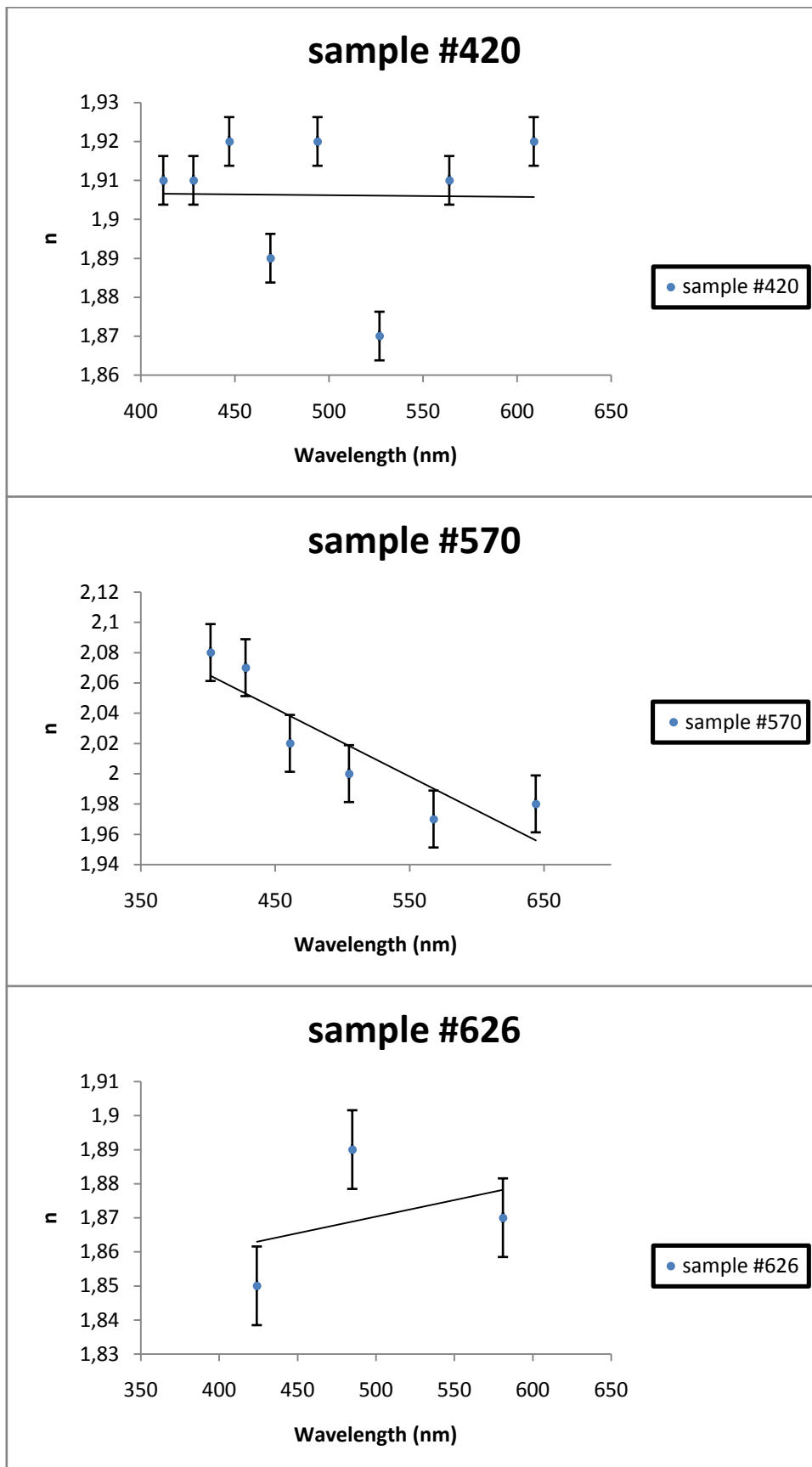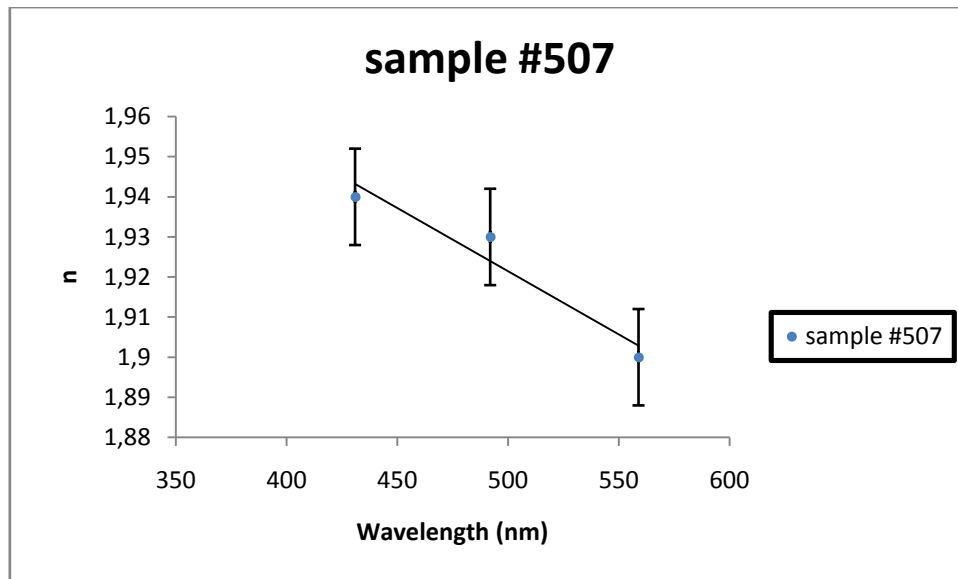
Fig. 4.3 *Refractive index for the films: a) sample #420, b) sample #570,*
c) sample #626, d) sample #507

As observed, for ZnO samples #420 and #626, refractive index n does not have major shifts, in the visible region of the wavelength; it has an average value of 1.89. For InO$_x$ samples #570 and #507, refractive index begins from a high value in the low visible region and slowly decreases as it progresses in the high visible region; it has an average value of 1.99.

For the verification of our calculated thickness, we compare it with the thickness obtained using the profilometer (A-step) technique. Although A-step is a precise technique, the thickness that we obtain using A-step for our metal oxide thin films, was in fact the average measurement of the values (of thickness), obtained by the stylus when it scans the surface. We use the average value because as it is known, the roughness of metal oxide thin films (ours too) surface, is not uniformed but dispersed. Calculated thicknesses compared with the thicknesses obtained by A-step technique are presented in **Table 4.5**

Table 4.5. Calculated thickness and thickness obtained by A-step technique

Run	Material	Thickness by A-step (nm)	Thickness calculated (nm)	Difference (%)
420	ZnO	1600	1556.219	2.7
570	InOx	1012	1031.672	1.9
626	ZnO	600	562.064	6.3
507	InOx	600	555.759	7.4

As observed there is a difference between the two measured thicknesses, experimental (A-step) and theoretical (calculated). For thin films with high thickness, difference is minimal (1-3 %), while in thin films with lower thickness, difference is higher (6-8%).

By using equation (4.5) we determine the extinction coefficient; **Table 4.6 – 4.7**

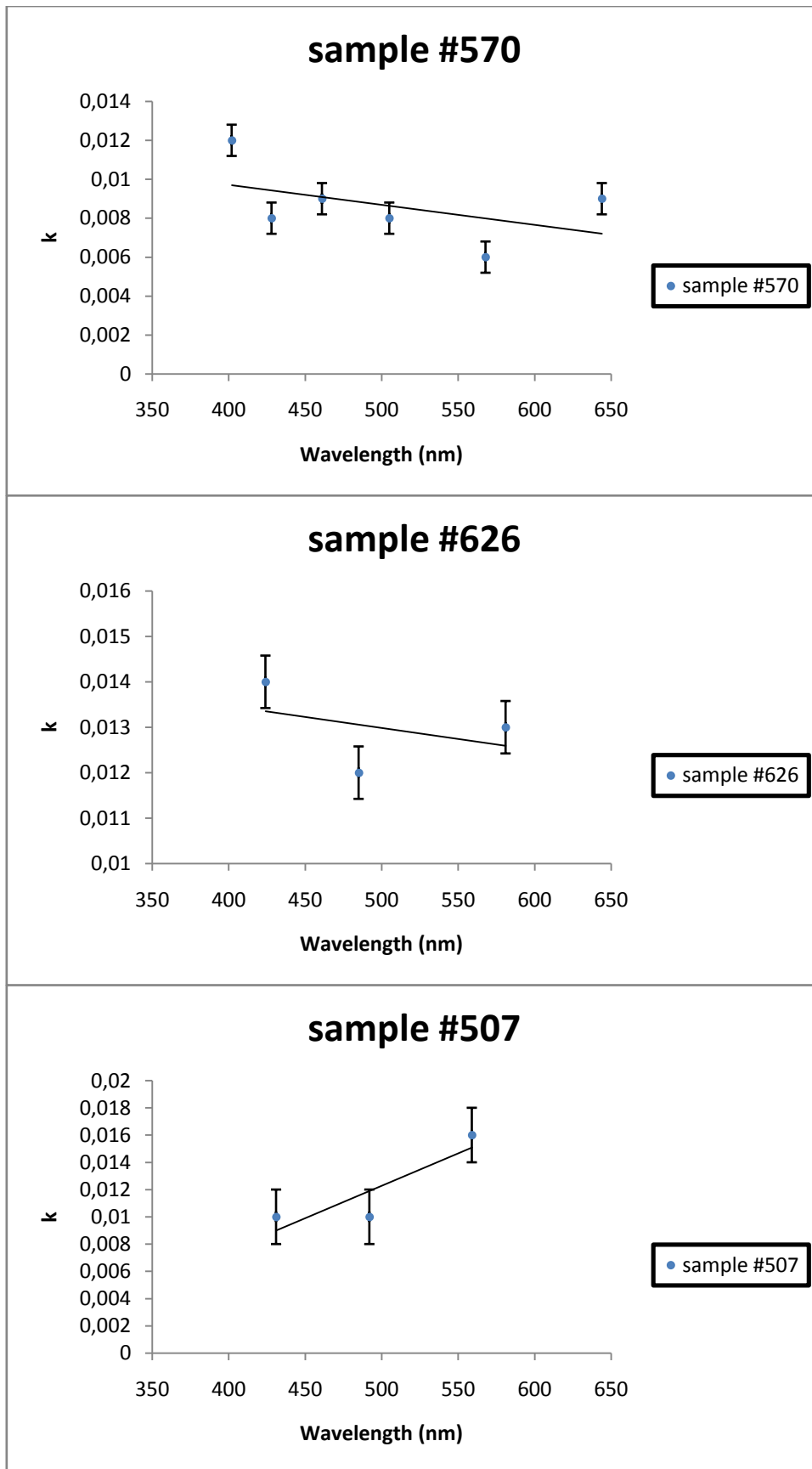**Table 4.6.** Extinction coefficient for samples **#420**, **#570**, **#626**, **#507**

Sample #420		Sample #570	
Wavelength (nm)	k	Wavelength (nm)	k
411.97	0.000	401.93	0.012
427.99	0.013	427.99	0.008
447.04	0.015	460.98	0.009
468.92	0.029	504.99	0.008
493.97	0.034	567.92	0.006
526.92	0.032	643.99	0.009
564.03	0.018		
608.92	0.008		

Table 4.7. Extinction coefficient for samples **#626**, **#507**

Sample #626		Sample #507	
Wavelength (nm)	k	Wavelength (nm)	k
424.01	0.014	430.97	0.010
484.95	0.012	491.98	0.010
581.05	0.013	558.97	0.016

In **Figure 4.4** we plot extinction coefficient versus wavelength:
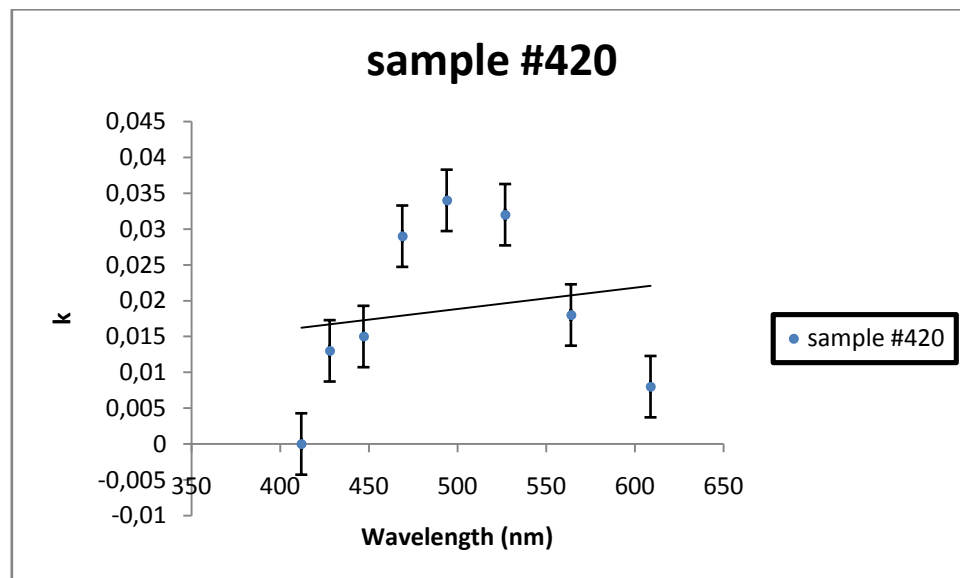
Fig. 4.4. Extinction coefficient for the films: a) sample #420, b) sample #570,
c) sample #626, d) sample #507

For sample #420, the extinction coefficient k has major shifts in the visible region, which is due to its large thickness (1600 nm); meaning that the surface of the sample has regions with high roughness, resulting in either more loss of light in certain wavelengths or allowance of the whole portion of light to get through. In our ZnO samples #420 and #626, the average value for the extinction coefficient is 0.018. For the InO_x samples #570 and #507, the average value is 0.011.

As it is known, values of refractive index n and extinction coefficient k in metal oxides, are not independent. Both of them are connected by the classical dispersion relations [38] for the complex dielectric function $\varepsilon \equiv \varepsilon_1 - i\varepsilon_2$:

$$n^2 - k^2 = \varepsilon_1 \tag{4.3}$$

$$2nk = \varepsilon_2 \tag{4.4}$$

ε_1 represents lattice permittivity, ε_L, of the material. Quantity 2nk is related to absorption. In Tables **4.6, 4.7, 4.8, 4.9** we present the calculated values of ε_1 (therefore ε_L) and ε_2.

Table 4.6 ε_1 and ε_2 calculation for sample #420

λ (nm)	n	k	ε_1	ε_2
411.97	1.91	0.000	3.648	0.001
427.99	1.91	0.013	3.648	0.049
447.04	1.92	0.015	3.686	0.057
468.92	1.89	0.029	3.571	0.109
493.97	1.92	0.034	3.685	0.130
526.92	1.87	0.032	3.495	0.119
564.03	1.91	0.018	3.647	0.068
608.92	1.92	0.008	3.686	0.030

Table 4.7 ε_1 and ε_2 calculation for sample #570

λ (nm)	n	k	ε_1	ε_2
401.93	2.08	0.012	4.326	0.049
427.99	2.07	0.008	4.285	0.033
460.98	2.02	0.009	4.080	0.036
504.99	2.00	0.008	4.000	0.032
567.92	1.97	0.006	3.881	0.024
643.99	1.98	0.009	3.920	0.036

Table 4.8 ε_1 and ε_2 calculation for sample #626

λ (nm)	n	k	ε_1	ε_2
424.01	1.85	0.014	3.422	0.052
484.95	1.89	0.012	3.572	0.045
581.05	1.87	0.013	3.497	0.049

Table 4.9 ε_1 and ε_2 calculation for sample #507

λ (nm)	n	k	ε_1	ε_2
430.97	1.94	0.010	3.763	0.039
491.98	1.93	0.010	3.725	0.038
558.97	1.90	0.016	3.61	0.061
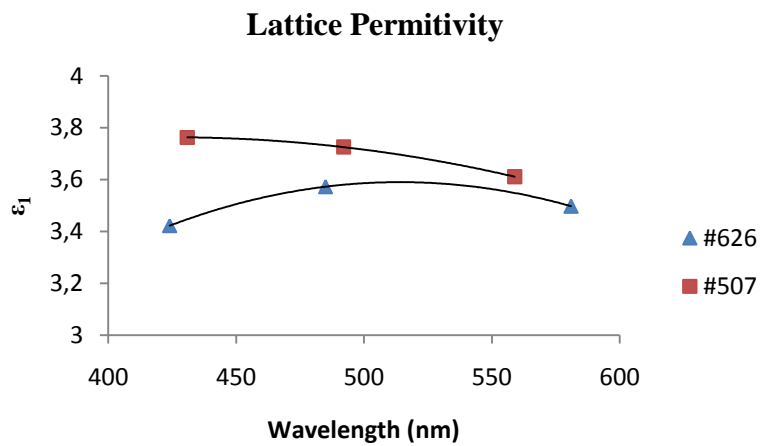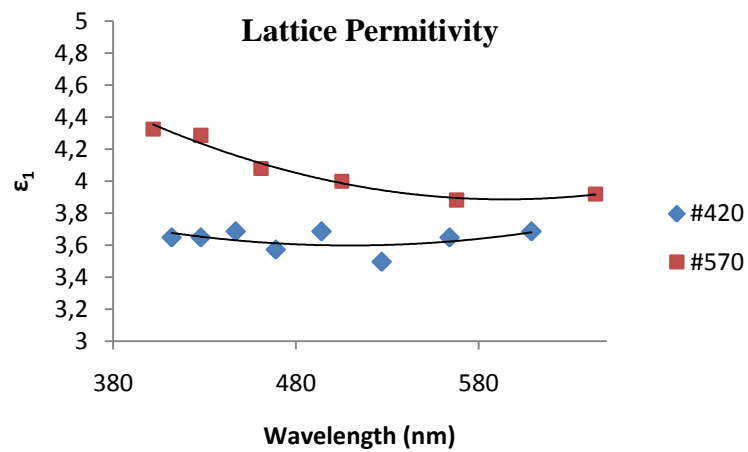
Fig. 4.5. *Real part (ε_1) of the complex dielectric function for our films*
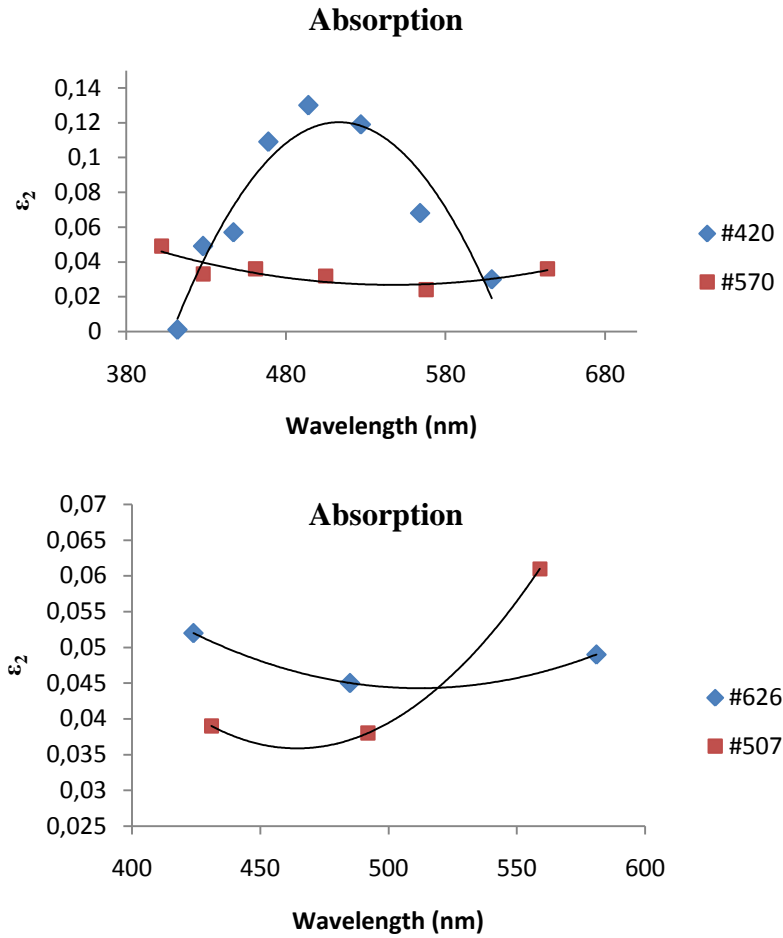
Fig. 4.6. *Imaginary part (ε_2) of the complex dielectric function for our films*

4.2.2 Optical band gap, E_g

Direct optical band gap of our deposited films was determined by optical measurements. For direct transitions between the edges of the parabolic bands, the fundamental absorption coefficient *a* is given by equation:

$$a = A\left(hv - E_g\right)^{1/2}$$

where E_g, is the optical band gap between valence and conduction band. Therefore, when we plot the a^2 versus *hv* and fit a straight light to the region above the edge we find the band gap, as can be seen in **Figure 4.7**.
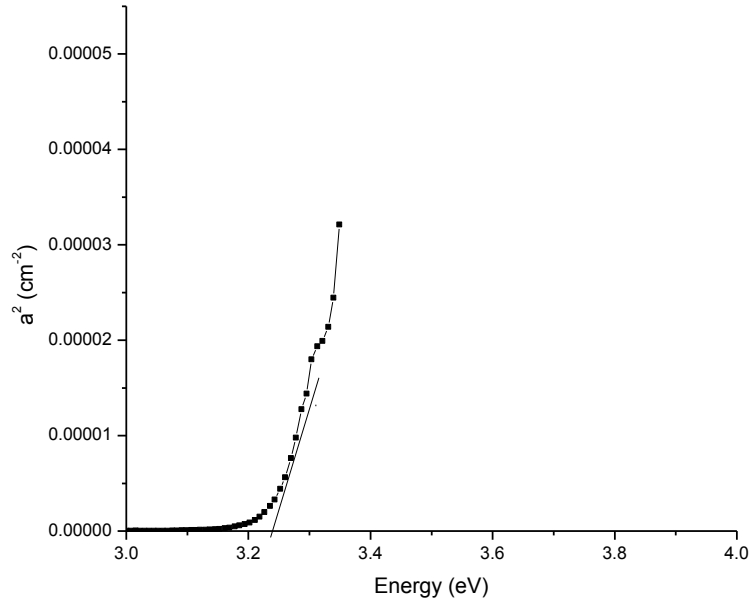
Fig. 4.7. a) Plot of a² versus hv (Energy) of our ZnO thin film sample #420

Band gap for our ZnO thin films #420 and #626, was calculated in the region of $E_g = 3.21 \pm 0.05$ eV, while for our InO_x films #570 and #507 was calculated in the region of $E_g = 3.50 \pm 0.05$ eV.

4.2.3 Discussion

The optical properties of InO_x and ZnO thin films, prepared by dc sputtering, have been studied for this section by optical transmission. Both Indium oxide and Zinc oxide were found to be transparent in the visible light region and to near infrared region, with a transmission range from 80% to 90%. For our Zinc Oxide films the refractive index average value is 1.89 and range from 1.86 to 1.92, while for our Indium Oxide we found that the refractive index average value is 1.99 and range from 1.92 to 2.08. The variation of the refractive index observed is mainly attributed to the oxygen absorbed after the deposition due to interaction of the surface with the atmosphere. This variation is also attributed to the surface roughness, which is to be expected for thin films prepared by dc sputtering. After obtaining the refractive index, we calculated the thickness of our films, comparing it also with the thickness determined by A-step.

We calculated, also, the extinction coefficient for each wavelength. Manifacier *et al.* [28] applied this method to SnO_2 films, prepared by spray and thermal evaporation techniques having a thickness of 900 nm and 2 μm, determining a relative error of around 2-5%. In our work, thickness was 600 nm, 1012 nm and 1600 nm and the calculation of n and k mostly have an error of around 4%.

With the values of n and k known, we calculate the lattice permittivity and the absorption of our films as a function of wavelength. For InO_x films, lattice

permittivity was found to be in the region of 3.6-4.3, while for ZnO is in the region of 3.3-3.8.

A direct optical band gap was found to be E_g=3.21±0.05 eV for ZnO films and E_g=3.50±0.05 eV for InO$_x$ films. The shift of the energy band gap has been attributed to Burstein-Moss effect **[39, 40]**.

As observed in Table 4.5, for thin film with thickness of 900 nm and above, the calculated thickness is in agreement with the thickness obtained by A-step technique, but for thin films with thickness lower than 1 μm is not. To determine the thickness of these thin films we use another method that was described in section 3.3, spectroscopic ellipsometry.

4.3 Spectroscopic Ellipsometry

4.3.1 Introduction

As stated in section 3.3, in SE we measure (ψ, Δ) values. Ψ is the amplitude ratio, while Δ is the phase difference of the p- and s- polarized light waves. In this work, samples were of Zinc oxide and the measurements were carried out in the ultraviolet/visible region, or from 1 eV to 6 eV region. Theoretical thickness of the samples used was 200 nm and 250 nm.

Data analysis consists mostly, of fitting our experimental data to a model, where certain parameters are used to obtain the best fit possible. Fitting process can be summarized in three steps [37]:

1) *Model selection/creation:* Input in this step is the number of layers, so the basic structure of our thin film is known; input of any interface layer as a single effective medium or more complicated interface
2) *Assign optical function to each layer:* Use of existing data or new parameterization.
3) *Fitting of the data:* Metric must be chosen that will decide between good and bad data fits.

Samples used for this work have 2 basic layers, corning glass as substrate (0.4 mm) and a thin layer that is our sample, ZnO. A hypothesis was made that between our thin film surface and ambient, there is an interference layer created by the oxidization of the surface when the sample came in touch with the atmosphere after the deposition. Optical constants for corning glass may be known, but for the purpose of this work (and because there is not any model known in the bibliography for it), a new model was created for it. In bibliography SE measurements were found for zinc oxide. The difference with our samples is that our substrate is of corning glass while the substrate used in bibliography was of Si; therefore a new model was made for the samples.
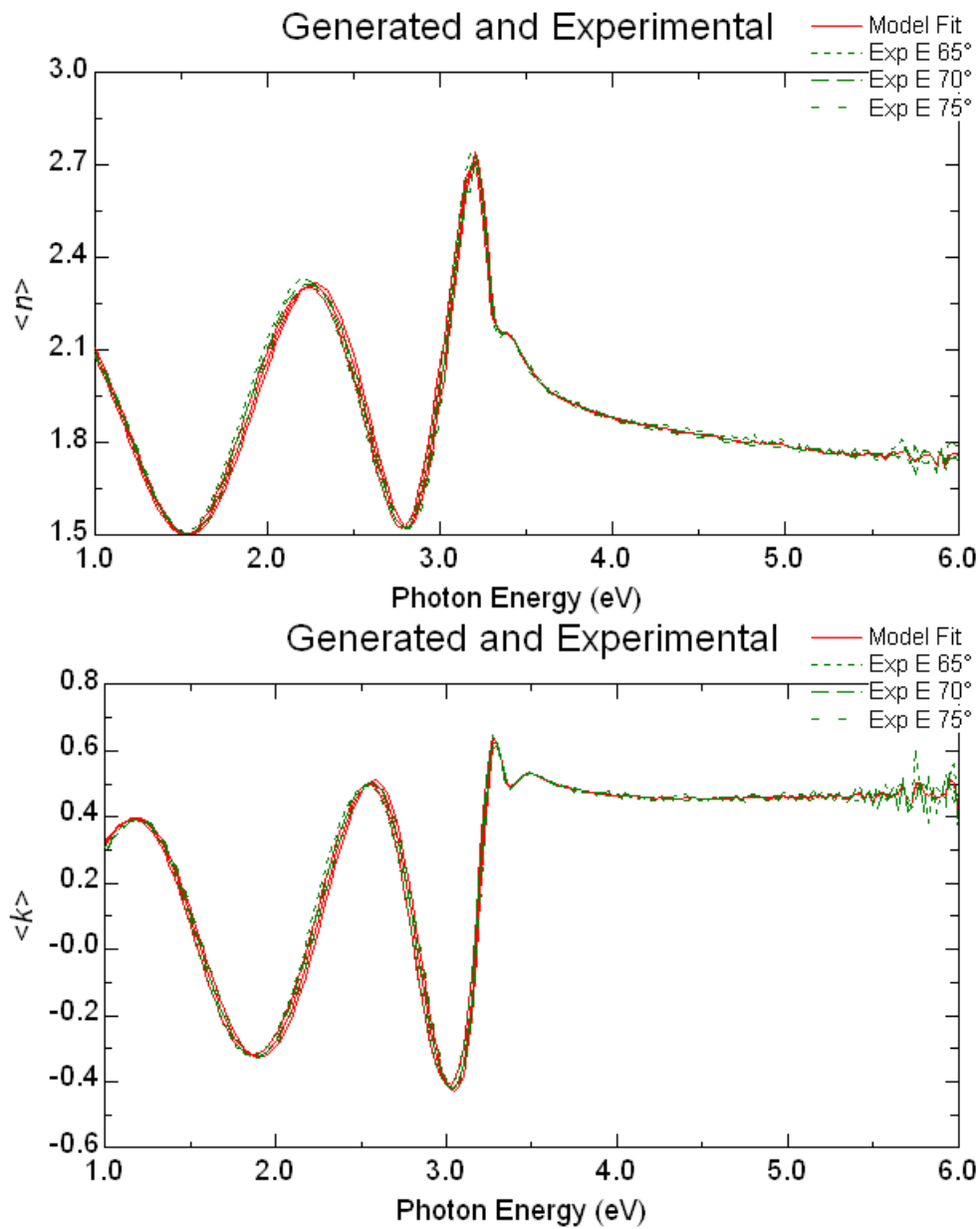
4.3.2 Data Analysis

Fitting of measured values (ψ, Δ) can be seen in **Figure 4.8**.
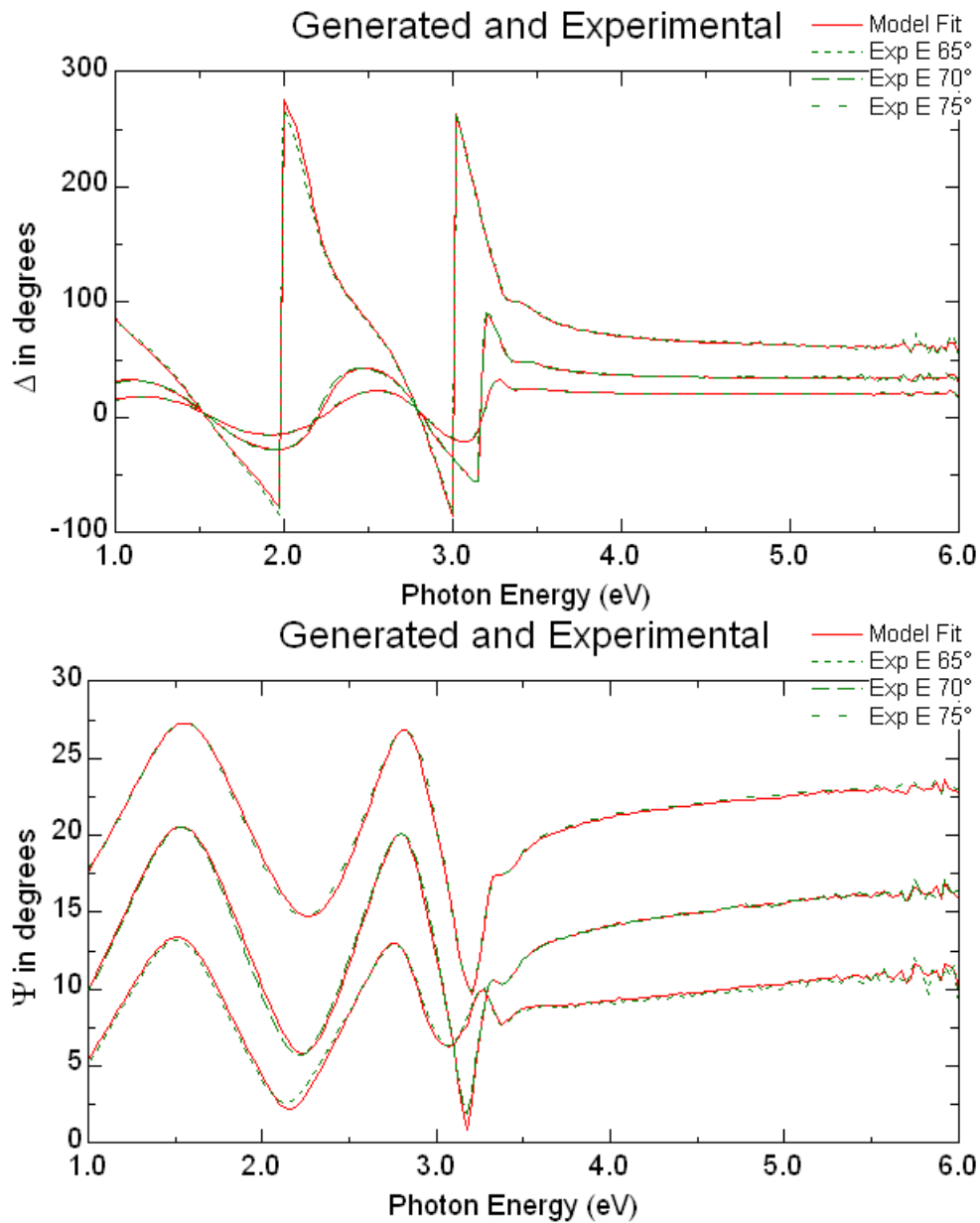

Fig. 4.8. *Fitting of values (ψ, Δ) of sample #497 (~250 nm)*

As observed in those fitted values, in the region 3.5 – 6 eV, there is full absorption from the thin film. In **Figure 4.9** the fitted values for refractive index and extinction coefficient can be seen.
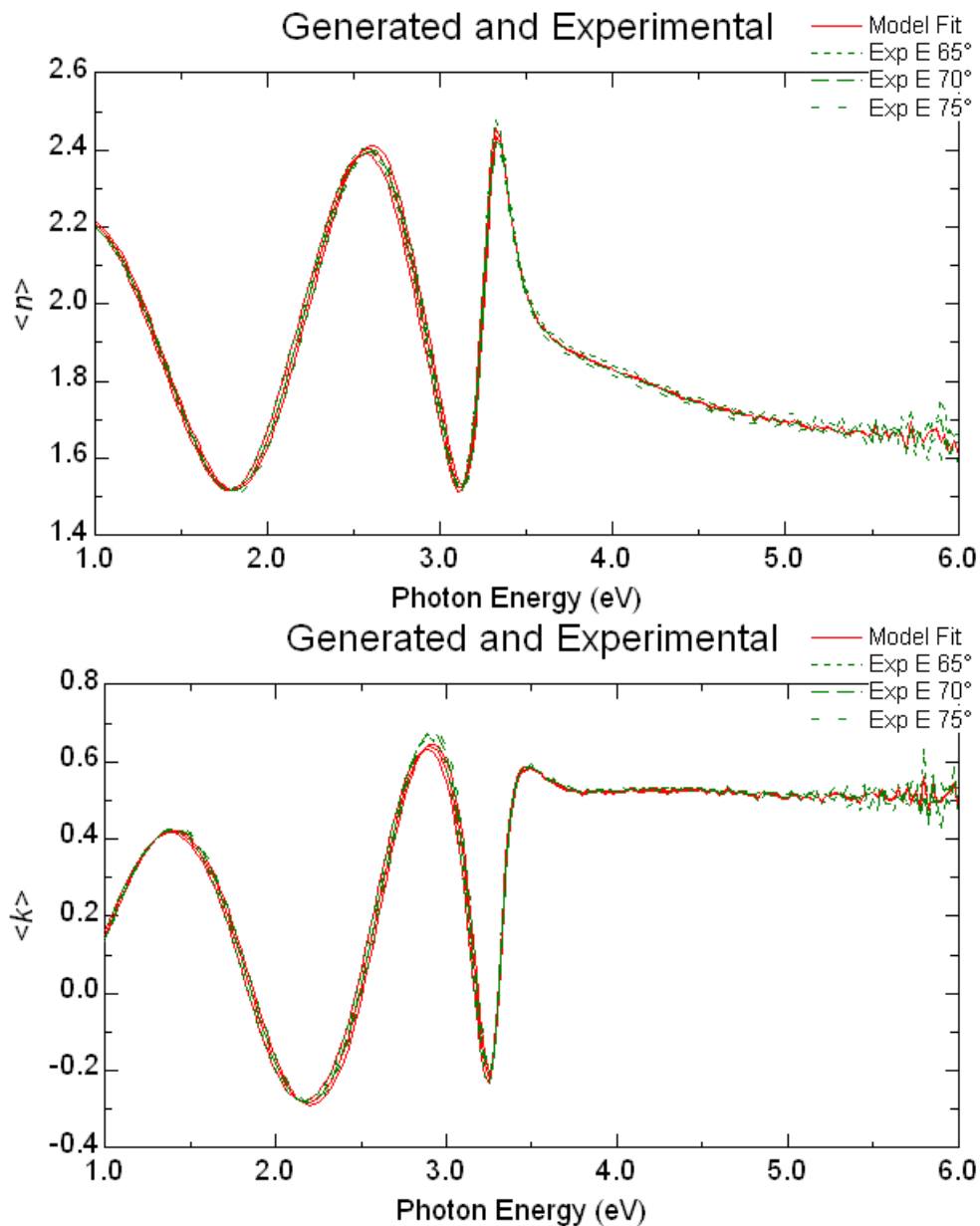
Fig. 4.9. *Fitted values of (n, k) for sample #497*

Those fitted values were of sample #497 with a thickness of 250 nm. For sample #590 fitted values can be seen in **Figure 4.10** and **Figure 4.11**.
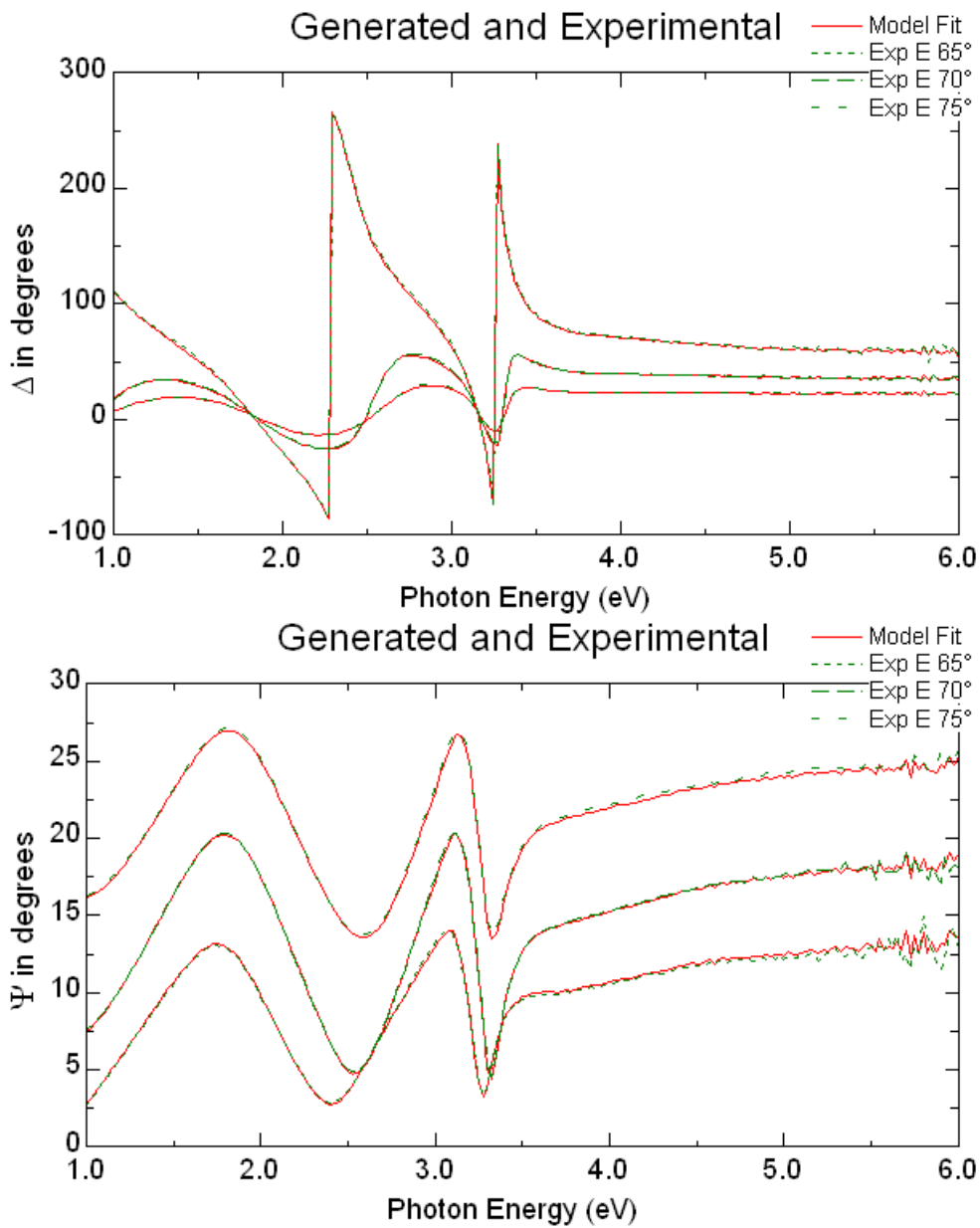
***Fig. 4.10.*** *Fitting of values (ψ. Δ) for sample #590 (200 nm)*

**Fig. 4.11.** *Fitting values (n, k) of sample #590*

The fitting values, shown in the figures above, are the overall for our samples; meaning the substrate-thin film- interference layer. In samples with thickness 200 nm and 250 nm, interference layer thickness was in the region of 5-8 nm, which is to be expected. In sample with thickness 510 nm, interference layer had a thickness of 20 nm.

In the models produced for the data analysis, modeling of n and k values was also made; **Figure 4.12**.
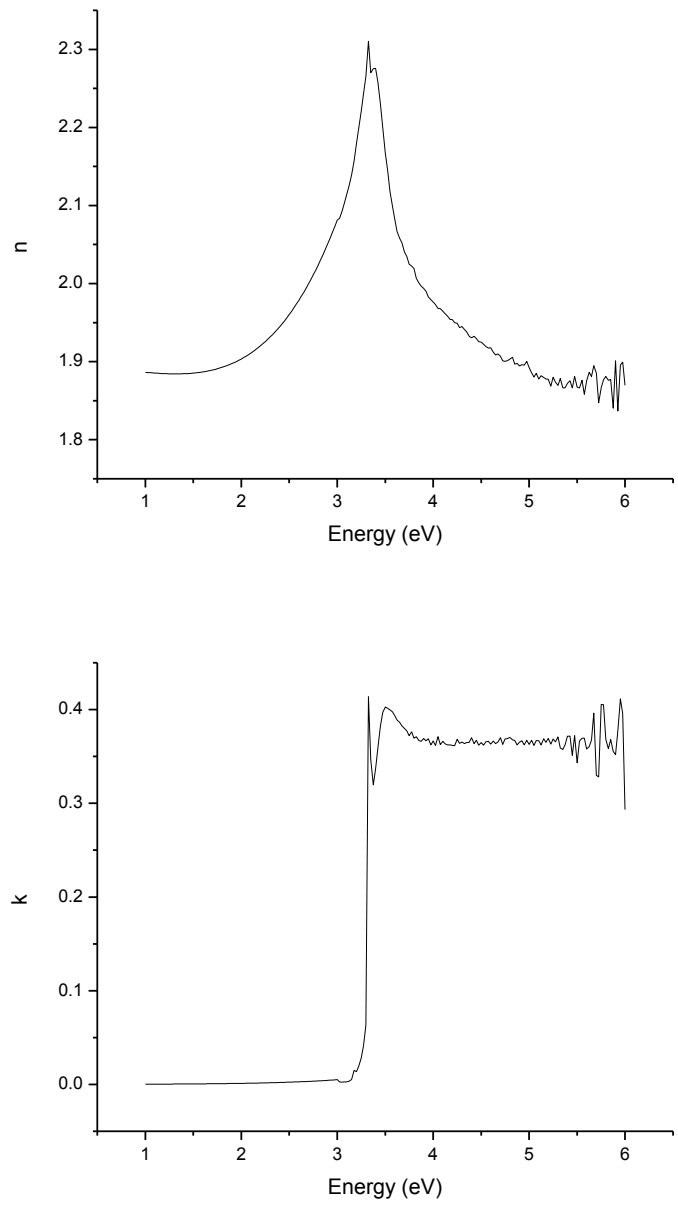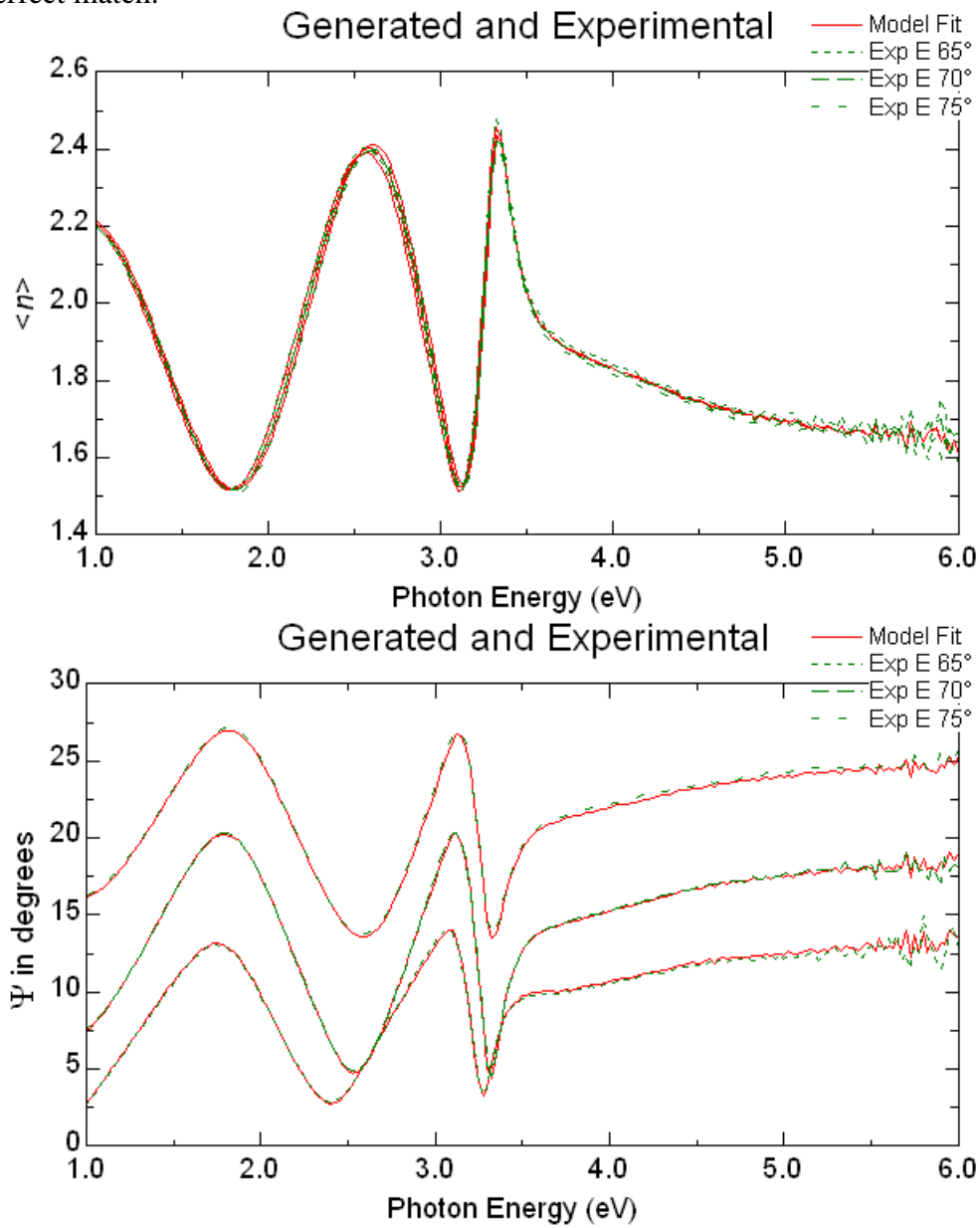

Fig. 4.12. Values of (n, k) for sample #497

In **Figure 4.13** values of (n, k) for sample #590 will be shown.
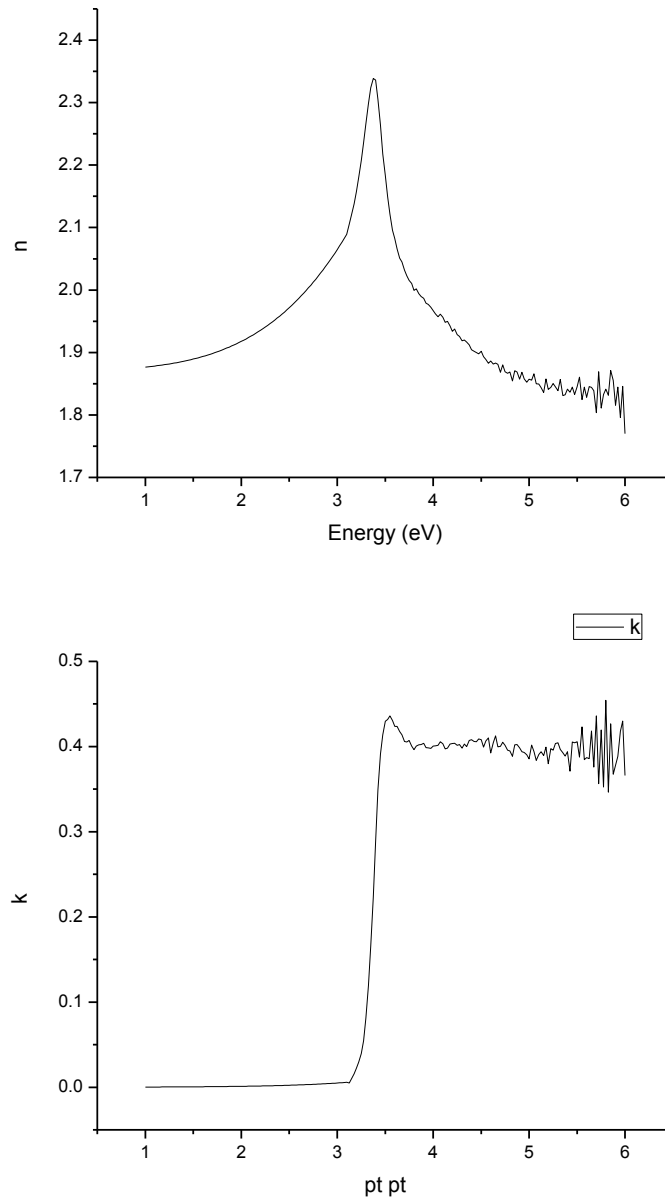

Fig. 4.13. Values of (n, k) for sample #590

As observed from the **Fig. 4.12** and **Fig. 4.13** the models of n, k for both samples are similar. To justify that those models are similar we will use the model of each one to fit the values of ψ, Δ for the other one.

Using the modeling of sample #497 to fit the values of ψ, Δ for sample #590 we have a perfect match.

Fig. 4.14. *Values of (ψ, Δ) for sample #590 using sample's #497 modelling*

Now we use the model of sample #590 to fit the values of ψ, Δ for sample #497.
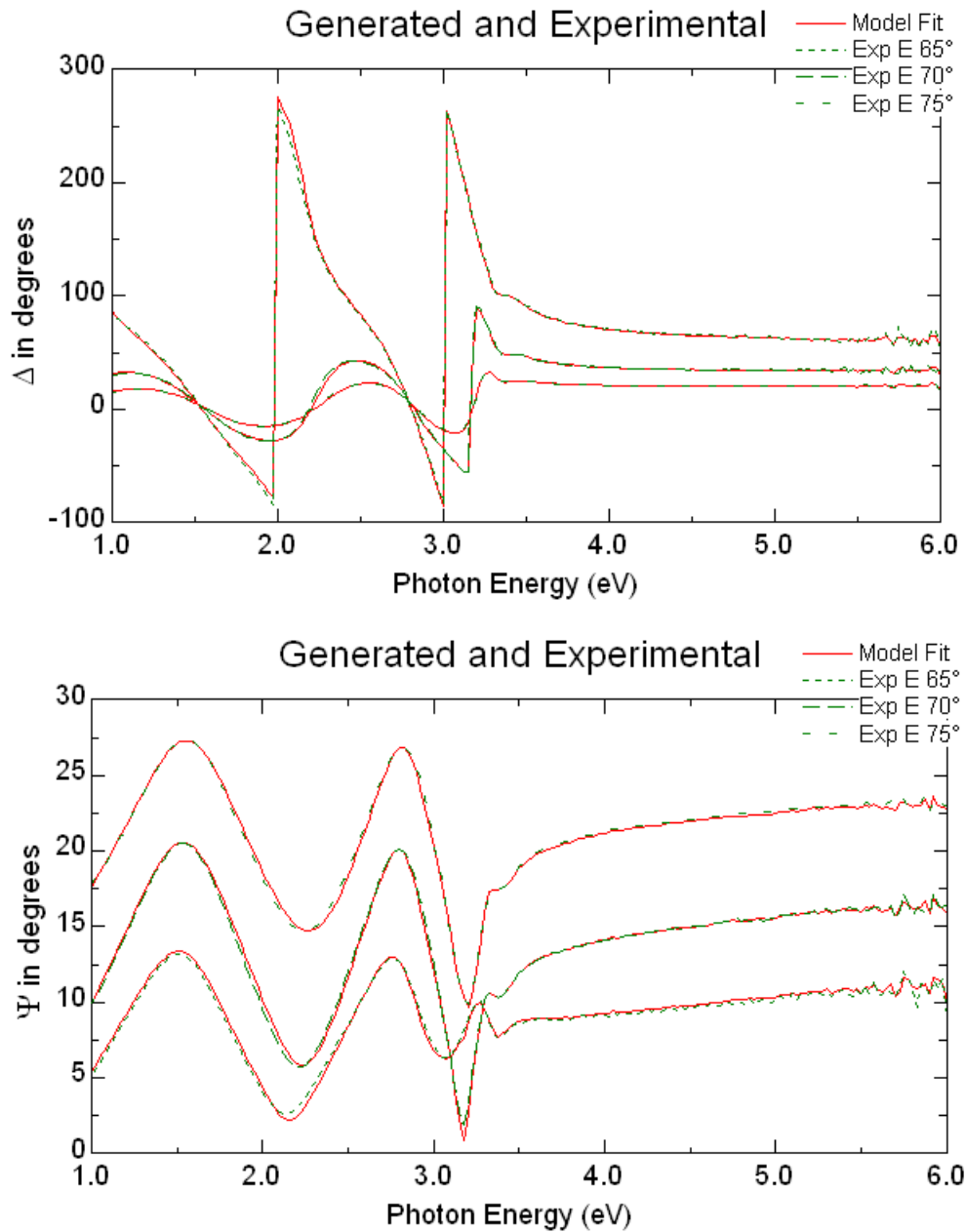
Fig. 4.14. *Values of (ψ, Δ) for sample #497 using sample's #590 modelling*

As observe in the **Fig 4.14**., usage of sample's #590 model has a perfect match for the fitting of values of ψ, Δ for sample #497.

4.3.3 Discussion

In this section we used spectroscopic ellipsometry in the region of 1 eV to 6 eV to determine the amplitude ratio (ψ), the phase difference (Δ), the refractive index (n) and the extinction coefficient (k) of our samples (#497 and #590). Our samples consist of 2 basic layers, the substrate (corning glass of 0.4 mm thickness) and a thin layer which is our sample, ZnO. We assumed that between the thin film surface and the ambient, a new layer was created by the oxidization of the surface when it came in touch after the deposition with the atmosphere.

Altough in biblography SE measurements were found for ZnO, the substrate of those samples were Si; therefore we created new models for the substrate and the sample. With the fitted values known we observed that in the region $3.5 - 6$ eV, there is full absorption from the thin film surface.

For the final part we used the modeling of n and k for each sample to fit the ψ, Δ values of the other sample. When the fitting for each sample was finished, the result was that either model could be used to fit the values needed for our work. Therefore we found a model for the fitting of ZnO (with corning glass as substrate) ψ, Δ values.

5.   GENERAL CONCLUSIONS

In this thesis, Zno and InO_x films with thicknesses of 200-1600 nm have been deposited by reactive dc magnetron sputtering technique using a 99.999% pure target onto room temperature substrates. We used a Perkin-Elmer UV/Vis transmission spectrometer and a spectroscopic ellipsometer to obtain the films spectra for measuring optical and structural properties.

For the first part of this thesis, two ZnO and two InO_x have been used. Spectra obtained by the Perkin-Elmer spectrometer were used for optical characterization, measuring refraction index n and extinction coefficient k, and for structural characterization, measurement of films thickness and energy gap. Refractive index of our Zinc Oxide films had an average value of 1.89 while for our Indium oxide films it had an average value of 1.99. The variations found in the measurements are attributed mainly to the fact that even after the deposition oxygen is absorbed due to the interaction of the films with the atmosphere and to the surface roughness of the films. With the refractive index known we calculated the thickness of our films using the method used by Manifacier *et al* [28] and then compared it with the thickness obtained using A-step. In our work, thickness of the films were 600 nm, 1012 nm and 1600 nm and the calculation of n and k gave us an error of around 4%. A direct optical band gap was found to be E_g=3.21±0.05 eV for ZnO films and E_g=3.50±0.05 eV for InO_x films. The shift of the energy band gap has been attributed to Burstein-Moss effect [39, 40].

For the second part of the thesis, two ZnO films have been used for spectroscopic ellipsometry measurements, to define ψ, Δ values as well as n, k values. Although in our samples there are two basic layers (substrate and the thin film), we assumed there is also another small one due to the oxidazation of the surface of our film. Modeling of the substrate was made due to the fact we did not find a similar one the known bibliography as well as modeling of our thin films. With the models known, we fitted the values of ψ, Δ and made a model for our refractive index, n, and extinction coefficient, k. For the final part we used the models we made for n and k of each sample to determine if we have a model that can be used for the fitting of ψ, Δ of the other sample and hopefully for ZnO thin films in general.

REFERENCES

1. E. Staritzky: Anal. Chem. **28**, 553 (1956)
2. M. Marezio: Acta Crystallogr. **20**, 723 (1966)
3. M. Marezio, A. Waintal, J. Chenavas, J.J. Capponi and M. Gondrand: Colloq. Int. Centr. Nat. Rech. Sci. **188**, 403 (1970)
4. "International Tables for X-ray Crystallography", *Vol. I: Symmetry Groups,* in p.315 (eds. N.F.M. Henry and K. Longdale), Kynoch Press, Birmingham, England, 1969
5. C.W. Bunn, Proc. Phys. Soc. London 47 (1935) 835
6. A. Tsukazaki, A. Ohtomo, T. Onuma, M. Ohtani, T. Makino, M. Smiya, K. Ohtani, S.F. Chichibu, S. Fuke, Y. Segawa, H. Ohno, K. Koinuma, M. Kawasaki, Nat. Mater. 4 (2005) 42
7. O. Dulub, L.A. Boatner, U. Diebold, Surf. Sci. 519 (2002) 201
8. J.C. Philips, Bonds and Bands in Semiconductors, Academic, New York, 1973
9. D.R Lide (Ed.), CRC Handbook of Chemistry and Physics, 73rd Edition, CRC Press, New York, 1992
10. E.H. Kisi, M.M. Elcombe, Acta Cryst. C45 (1989) 1867
11. J.E. Jaffe, A.C. Hess, Phys. Rev. B 48 (1993) 7903
12. L. Gerward, J.S. Olsen, J. Synchrotron Radiat. 2 (1995) 233
13. C.H. Bates. W.B. White, R. Roy, Science 137 (1962) 993
14. M. Zamfirescu, et al., Phys. Rev. B **65** 161205 (2002)
15. . O'Kane, Phys. Rev. B **18**, 6849 (1978)
16. D.S. Chemla and J. Shah, Nature **411**, 549 (2001)
17. J.H.W. de Wit: J. Sol. Stat. Chem. **13**, 192 (1975)
18. W.H. Hirschwald, Acc. Chem. Res., **1985**, 18(8), pp 228-234 (1985)
19. P. Kofstad: "Non-stoichiometry, Diffusion and Electrical Conductivity in Binary Metal Oxides", Wiley, New York, 1972
20. G. Kiriakidis, M. Suchea, S. Christoulakis and N. Katsarakis: "High Performance gas sensing materials based on nanostructured metal oxide films", Review on Advanced Materials Science 10. 2005 215-225
21. G. Kiriakidis, H. Ouacha and N. Katsarakis: "Nano-structured metal oxide films with room temperature gas sensing properties", NATO Science Seires II: Mathematics, Physics and Chemistry, Kluwer Academic Publishers, Dordrecht, Volume 128, p. 363-382, 2003
22. J.L. Vossen and J.J. Cuomo: *"Thin Film Processes",* ed. J.L. Vossen and W.Kern, Academic Press, New York, 1978
23. W.D. Westwood: *"Microelectronic Materials and Processes",* ed. R.A. Levy, Kluwer Academic, Dordrecht, 1989
24. B.N. Chapman: *"Glow Discharge Processes"*, Wiley, New York, 1980

25. M. Ohring: *"The Materials Science of Thin Films"*, chap. 3: *"Physical Vapour Deposition"*, Academic Press, San Diego, 1992

26. A. Mannan, Growth and study of magnetostrictive FeSiBC thin films, for device applications, 1999

27. A.M. Goodman: App. Opt. **17**, 2779 (1978)

28. F.A. Jenkins and H.E. White: *"Fundamentals of Optics"*, p. 255. McGrow-Hill, New York, 1950

29. J.C. Manifacier, J Gasiot and J.P. Fillard: J. Phys. E **9**, 1002 (1976)

30. J.C. Manifacier, J Gassiot, J.P. Fillard and L. Vicario: Thin Solid Films **41**, 127 (1977)

31. J.I. Pankove: *"Optical Processes in Semiconductors"*, Dover New York, 1971

32. E. Burstein: Phys. Rev. **93**, 632 (1954)

33. T.S. Moss: Proc. Phys. Soc. **B76**, 775 (1954)

34. D. E. Aspnes and A.A. Studna, High precision scanning ellipsometer, *Appl. Opt.,* **14** (1975) 220-228

35. R.H Muller and J.C. Farmer Fast, self compensating spectral-scanning ellipsometer, *Rev. Sci. Instrum.,* **55** (1984) 371-374

36. Y.Y. Kim, R.W. Collins and K. Cedam, Fast scanning spectroelectrochemical ellipsometry: in-situ characterization of gold oxide, *Surf. Sci.,* **233** (1990) 341-350

37. R.M.A. Azzam and N.M. Bashara, *Ellipsometry and Polarized Light,* North Holland, Amsterdam (1977)

38. H.G. Tompkins and W.A. McGahan, *Spectroscopic Ellipsometry and Reflectrometry: A User's Guide,* John Wiley & Sons Inc., New York (1999)

39. H.G. Tompkins and E.A. Irene, Eds, *Handbook of Ellipsometry,* William Andrew, New York (2005)

40. A.H. Clarc: *"Properties of Polycrystalline and Amorphous Thin Films and Devices"*, Chap. 4:*"Optical Properties of Polycrystalline Semiconductor Films"*, Academic Press, New York, 1980

41. J. Szczyrbowski, K. Schmalzbauer and H. Hoffmann: Thin Solid Films **137**, 169 (1986)

42. H. Nanto, T. Minami, S. Shooji and S. Takata: J. Appl. Phys, 1029 (1984)

43. J.I. Pankove, *Optical Process in Semiconductors*, Dover Publications, New York (1971)

44. S. Adachi, *Optical Properties of Crystalline and Amorphous Semiconductors, Materials and Fundamental Principles*, Kluwer Academic Publishers, Norwell (1999)